

1 **Enhanced net CO₂ exchange of a semi-deciduous forest**
2 **in the southern Amazon due to diffuse radiation from**
3 **biomass burning**

4 **S. N. R. Silva¹, G. G. Cirino^{2,1,5}, D. S. Moreira³, R. S. Palácios^{2,5}, M. I.**
5 **Vitorino^{1,2}, and G. L. Vourlitis⁴**

6 ¹Programa de Pós-Graduação em Ciências Ambientais, Universidade Federal do Pará, Belém-PA, Brazil

7 ²Instituto de Geociências, Faculdade de Meteorologia, Universidade Federal do Pará, Belém-PA, Brazil

8 ³Faculdade de Ciências, Universidade Estadual Paulista, Bauru-SP, Brazil

9 ⁴Department of Biological Sciences, California State University, San Marcos, CA, USA

10 ⁵Programa de Pós-Graduação em Gestão de Risco e Desastre na Amazônia, Universidade Federal do

11 Pará, Belém-PA, Brazil

12 **Key Points:**

- 13 • Enhancement up to 40% in the diffuse PAR for high aerosols loading ($AOD \geq 1.25$)
14 • Enhancement up to 20-70% in the NEE of CO₂ for high aerosols loading ($AOD \geq 1.25$)
15 • Photosynthetic interruption for relative irradiance values below 60%
16 • Decrease in the NEE of CO₂ for canopy temperature values below 25 °C
17 • Decrease in the NEE of CO₂ for VPD values below 3-4 hPa

Corresponding author: G. L. Vourlitis, georgev@csusm.edu

Abstract

Atmospheric processes and climate are closely linked to the carbon cycle in the Amazon region as a consequence of the strong biosphere-atmosphere coupling. The radiative effects of aerosols and clouds are still unknown for a wide variety of species and types of vegetation present in Amazonian biomes. This study examines the effects of atmospheric aerosols on solar radiation and their effects on Net Ecosystem Exchange (NEE) in an area of semideciduous tropical forest in the North of Mato Grosso State. Our results show a reduction of assimilation in the NEE with a considerable loss with the decrease of incident solar radiation of $\approx 40\%$ and relative irradiance between 1.10-0.67. An average increase of 35-70% in net CO_2 assimilation was observed for pollution levels (Aerosol Optical Depth) above ≈ 1.25 . The increase of 35-70% in the NEE was attributed to the increase of up to 60% in the diffuse fraction of Photosynthetically Active Radiation concerning its direct fraction. These results were mainly attributable to the Biomass Burning Organic Aerosols from fires over the area studied. Important influences on temperature and relative humidity of air induced by the interaction between solar radiation and high aerosol load in the observation area, were also observed; an average cooling of $\approx 3.0^\circ\text{C}$ and 10%, respectively. Given the long-distance transport of aerosols emitted by burning biomass, significant changes in CO_2 flux can be occurring over large areas of the Amazon, with important effects on the potential for CO_2 absorption on ecosystems of semideciduous forests distributed in the region.

Plain Language Summary

Here, first we obtained clear-sky curves with the AOD measurements from the AERONET sun photometer network. Next this, the radiative effects of aerosols on the CO_2 fluxes for experimental site were analyzed. Measurements of NEE, total PAR radiation (PAR_i), diffuse PAR radiation (PAR_d), (AOD_a), (RH_{air}), (T_{air}) and surface temperature of the forest canopy (T_{df}) were further analyzed as a function of the relative irradiance parameter (f), from July to November, during the burnign season in the region.

1 Introduction**1.1 Scientific Contextualization**

Carbon is a key element in global biogeochemical cycles. Understanding its balance is fundamental to understanding the interactions between life (bio) the earth (geo) and chemistry. In the current context of global climate change, the modulating agents of CO_2 stocks and fluxes, especially through photosynthesis-respiration processes, have been widely debated (Booth et al., 2012; Huntingford et al., 2013; Brienen et al., 2015) with emphasis on the role of tropical forests, especially for the Amazon (Doughty et al., 2015; Braghieri, Kerches Renato, Akemi Yamasoe et al., 2020; Gatti et al., 2014, 2021). The result of increasing atmospheric CO_2 levels associated with climate change provides important feedback on the future of greenhouse warming (Booth et al., 2012; Huntingford et al., 2013).

In the Amazon biome, forest ecosystems play an important role in the dynamics between the carbon cycle of the terrestrial component and the climate, and even if these forests seem to have a uniform behavior, they have climatic sub-regions with peculiarities for the process of absorption and release of carbon (Brienen et al., 2015; Gatti et al., 2021). The absorption, carried out through photosynthesis, increases the stock of CO_2 fixed by the vegetation, incorporating this component as a biomass gain, that is, a carbon sink. The process of respiration of vegetation and soil releases CO_2 into the atmosphere, that is, a source of carbon for the atmosphere. Photosynthesis and respiration processes can vary considerably from sub-region to sub-region in Amazonia, resulting in

66 distinct carbon source or sink behaviors depending on geographic location and climatic
67 conditions (Doughty et al., 2015; Silva et al., 2020).

68 In general, the participation of forests in the global carbon cycle can only be ad-
69 equately quantified by long-term studies monitoring carbon exchange at the plant-atmosphere
70 interface. Forests participate in this cycling effectively, storing 200-300 Pg C (Pan, 2011;
71 Saatchi et al., 2011; Avitabile et al., 2016), about a third of what is contained in the at-
72 mosphere. This stock is very dynamic and these trees process about 60% of global pho-
73 tosynthesis, sequestering about 72 Pg C from the atmospheric component every year (Beer
74 et al., 2010), but also releasing a similar amount back into the atmosphere via respira-
75 tion of plants and animals, microorganisms and fungi of the (R. C. Nagy et al., 2018)
76 ecosystem. In these large fluxes, a small proportionate change in the uptake or release
77 of CO₂ to the atmosphere can result in a large net source or sink.

78 Changes in carbon concentrations in the atmosphere since the industrial era directly
79 impact the role of forest in carbon cycles, which can alternate between the source or sink
80 of CO₂. Recent reports (Gatti et al., 2021) show that some regions of the Amazon act
81 as a source of CO₂ to the atmosphere, as a result of logging, land use change, and fires
82 that occur in the region. However, other research indicates that Amazonian forests can
83 be net sinks for atmospheric CO₂ (Carswell et al., 2002; von Randow et al., 2004) or ap-
84 proximately in balance (Vourlitis et al., 2011). In general, the balance between the rates
85 of carbon emission or fixation is delicate, so small external disturbances can change the
86 dynamics of the forest and the state of the climate system.

87 Among the modulating agents of the CO₂ balance, solar radiation stands out, as
88 a fundamental component for both photosynthesis and forest respiration. In Brazil, and
89 especially in the Amazon region, the burning of biomass emits large amounts of gases
90 and aerosols into the atmosphere, these emissions can strongly alter radiative fluxes, im-
91 pacting CO₂ (Aragão et al., 2018; Malavelle et al., 2019; Morgan et al., 2019; de Mag-
92 alhães et al., 2019). Atmospheric aerosols from biomass burning intimately affect the light
93 use efficiency (*LUE*) and ecosystem productivity, influencing the solar radiation received
94 in the system and other exogenous environmental conditions (Kanniah et al., 2012; Mer-
95 cado et al., 2009). Studies of the effects of aerosols carried out on terrestrial ecosystems
96 have found positive, negative, and neutral effects. In Amazonia, these effects were also
97 observed in some regions, such as in the central part (G. G. Cirino et al., 2014), east (Doughty
98 et al., 2010; Oliveira et al., 2007) and southwest (Yamasoe et al., 2006; G. G. Cirino et
99 al., 2014), but remain unknown in critically important ecosystems, such as seasonal forests
100 (in the region of the deforestation arc), Pantanal forests, woodlands and cerrado. Mod-
101 eling studies have also demonstrated the impact of aerosols on gross primary production
102 (GPP) on a regional (Moreira et al., 2013; Bian et al., 2021) and global (Mercado et al.,
103 2009; Rap, 2015) scale.

104 The models used in these studies, however, need improvements in the physical pa-
105 rameterization of the radiative effects of aerosols and clouds, direct long-term observa-
106 tions in these ecosystems. These improvements are fundamental for more accurate and
107 realistic spatialization of the potential for the absorption of atmospheric CO₂ by the Ama-
108 zon as a whole (Aragão et al., 2018). In this sense, the potential for fire-induced atmo-
109 spheric aerosols to impact to CO₂ absorption by the seasonal forest in Mato Grosso (in
110 the region of the deforestation arc), has not yet been evaluated, either by direct obser-
111 vation or by numerical modeling. It is known that these tropical semideciduous forests
112 play a central role in the terrestrial system, preserving biodiversity (Fu et al., 2018). This
113 biome, located on the frontier of deforestation, is an excellent laboratory to assess the
114 effects of exogenous factors on forest productivity, as it is under strong anthropic impact
115 due to changes in land use, destined for the advancement of soy monoculture, livestock,
116 and the timber industry, as well as high vulnerability to fire. These are areas with a great
117 diversity of plant and animal species, essential for the cycling of nutrients and oxygen
118 and, therefore, for humans.

119 This research focuses on studying the action of biomass burning aerosols in an area
 120 of semi-deciduous forest located in the southern portion of the Amazon Basin, in the north
 121 of the State of Mato Grosso, in the region of the arc of deforestation, contributing to a
 122 better understanding of the cycle of carbon in the region. To this end, we specifically
 123 seek to: (1) develop a clear-sky irradiance algorithm using a long observation period of
 124 AOD_a ; (2) quantify the increase in the diffuse fraction of solar radiation at the expense
 125 of the presence of aerosols from fires in the experimental study area; (3) quantify net and
 126 relative changes in carbon fluxes through net ecosystem productivity (NEE of CO_2);
 127 (4) to evaluate the influence of fires on biophysical variables that influence forest pho-
 128 tosynthetic rates (Td_f , T_{air} and Vapour-Pressure Deficit). Aerosol data and microm-
 129 eteorological measurements in combination with carbon fluxes measured by the eddy co-
 130 variance system are used in the period 2005-2009. All solar radiation measurements are
 131 evaluated in terms of aerosol data (AOD_a), solar zenith angle (SZA), and relative ir-
 132 radiance f .

133 2 Data and Methods

134 2.1 Site descriptions

135 An area of transitional (semi-deciduous) tropical forest located in the south of the
 136 Amazon basin, 50 km northeast of Sinop, in the municipality of Cláudia (Lat $11^\circ 24.75'$
 137 S, Long. $55^\circ 19.50'$ W), in the State of Mato Grosso (Figure 1). This forest is located
 138 in the arc of deforestation, a region of continuous agricultural expansion, logging, and
 139 fires; (Nepstad et al., 2014; Balch et al., 2015; Alencar et al., 2022) (Figures S1, S2, and
 140 S3).

141 Previous studies report the peculiar characteristics of this type of forest; trees with
 142 lower height, biomass, and floristic diversity compared to humid tropical forests (Murphy
 143 & Lugo, 1986; Nogueira et al., 2008) due to their well-defined seasonal period (dry and
 144 rainy). The forest is 423 m above sea level, in a transition where the vegetation consists
 145 of savannah (cerrado), transitional vegetation (cerradão), and Amazonian forest, with
 146 some parts to the south of the Amazon Basin, near Sinop, recognized as dry forest or
 147 semideciduous (Ackerly et al., 1989; Ratter et al., 1978).

148 The deciduous and semi-deciduous forests within the Cerrado domain, initially cov-
 149 ered over 49.95 km^2 in the state of Mato Grosso, but currently 20.50 km^2 of this area
 150 is deforested ($\approx 41\%$), and only 14% is located within protected areas (Alencar et al.,
 151 2022). The geographic positions of these forests are discontinuous, due to climatic fluc-
 152 tuations that have occurred in the last 10,000 years (Prado & Gibbs, 1993). The tree
 153 species at this location are typical of the semi-deciduous forest of the Amazon, with max-
 154 imum canopy heights varying between 25-28 m. Comprehensive description of the species
 155 reported in the region was reported by Ackerly et al. (1989), Lorenzi (2000) and Lorenzi
 156 (2002). The soils are acidic with a pH measuring 4.2 and sandy (94% sand), well-drained
 157 quartzarenic neosols, poor in nutrients, and with low organic matter (Vourlitis et al., 2001;
 158 Oliveira-Filho AT & Oliveira, 2002), with a dry season that extends from May to Septem-
 159 ber (Vourlitis et al., 2002).

160 The 30-year average annual temperature in this area is 24°C , with precipitation
 161 of approximately 2000 mm/year (Vourlitis et al., 2002). Among the active atmospheric
 162 systems are the Bolivian High (BH), South Atlantic Convergence Zone (SACZ), and frontal
 163 Systems. To the north, the region is influenced by systems that operate in the Amazon,
 164 and the southern portion is affected by extratropical systems, such as frontal systems
 165 (Amorim Neto et al., 2015; Saraiva et al., 2016). The loss of leaves (deciduousness) dur-
 166 ing the dry season (July-September) is quite sensitive to water availability and temper-
 167 atures (maximum and minimum) in the region. With the arrival of the rainy season (November-

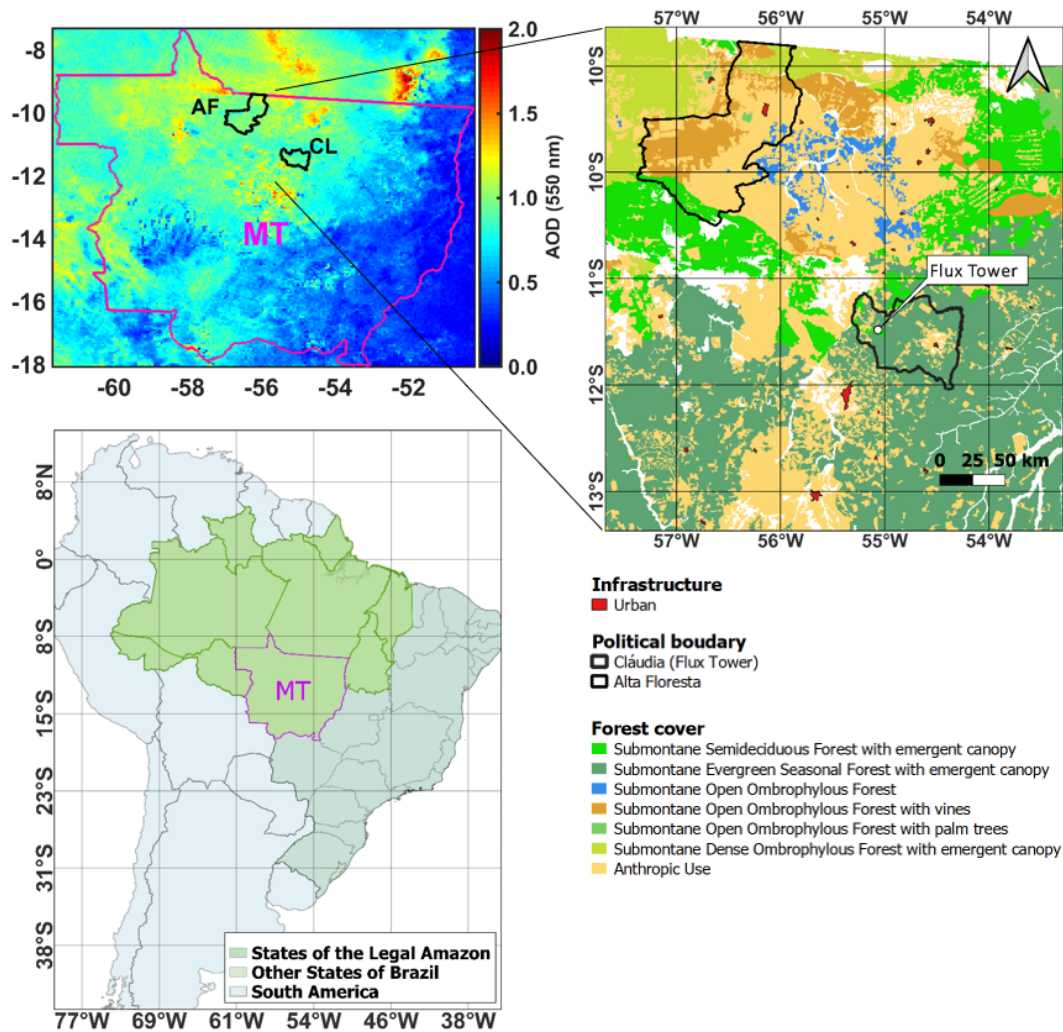


Figure 1. Localization map of micrometeorological tower in the Cláudia municipality, 50 km northeast of Sinop, Mato Grosso (white point, in the right pane).

168 May), the vegetation recovers again with typical characteristics of tropical forests (Vourlitis
 169 et al., 2011).

170 2.2 Instrumentation and Data

171 2.2.1 Aerosol Measurements

172 This study used a long series of aerosol optical depth measurements - AOD (Aerosol
 173 Optical Depth) to assess the impact of atmospheric particles on the flux of solar radi-
 174 ation to the surface. Two types of remote sensors were used: the MODIS (Moderate Res-
 175 olution Imaging Spectroradiometer) orbital sensor, available on board the AQUA and
 176 TERRA satellites, products MOD04-3K and MYD04-3K (Remer et al., 2013); and an
 177 AERONET (Aerosol Robotic Network) solar photometer, used as a standard measure
 178 of optical properties of atmospheric aerosols at the surface, between June1993-March2018
 179 (Holben et al., 1998). All remote aerosol information required for this study was oper-
 180 ated and maintained by NASA (National Aeronautics and Space Administration).

181 The TERRA /AQUA satellites have a heliosynchronous polar orbit with a Local
 182 Time (LT) of passage over the study areas around 10h30min and 13h30min. These space
 183 platforms cover the Earth’s surface every 1-2 days with radiance measurements in 36 spec-
 184 tral bands. The MOD/MYD043K aerosol products also feature the most current collec-
 185 tion of data available from NASA, currently at 3 Km spatial resolution for AOD and other
 186 aerosol optical properties (Levy et al., 2013; Remer et al., 2013). Filters to exclude con-
 187 tamination of data by clouds are also applied during estimation processing. The AOD
 188 series from these satellites has 20 years of data on continents and oceans and is widely
 189 available on the open access platform of the Atmospheric Files Distribution System - Level
 190 1, located at the Distributed Active Files Center (LAADS-DAAC) from Goddard Space
 191 Flight Center - GSFC, in Greenbelt, Maryland (USA). In this work, satellite AOD spa-
 192 tializations were used to obtain regional information on the nature or type of aerosol act-
 193 ing over the study area, between 2002-2020 (Figure S4). More detailed information about
 194 the MODIS sensor, such as spectral models, validation, and operating period of the afore-
 195 mentioned products can be found in (Remer et al., 2005, 2013).

196 Regarding seasonal forests in northern Mato Grosso, in Alta Floresta, a long se-
 197 ries of AOD measurements (> 20 years of data) are available through CIMEL Electron-
 198 ionic solar photometers, maintained and operated by NASA (GSFC), through the AERONET
 199 network (1993-2021). This photometer network is intended for the monitoring and char-
 200 acterization of aerosol particles in various regions of the world. These sensors represent
 201 the standard measure of AOD and are widely used in the validation of satellite AOD es-
 202 timates. The system operates solar radiation measurements and rotational interference
 203 filters to extract optical properties from aerosols in various spectral bands, between 340-
 204 1020 nm (Schafer, Holben, et al., 2002; Schafer, Eck, et al., 2002; Procopio et al., 2004;
 205 Schafer et al., 2008). This makes it possible to evaluate the direct influence of atmospheric
 206 particles in real time on regions highly affected by fires, such as the region of the arc of
 207 deforestation. In this work, AOD was used at wavelengths of 500 nm (AERONET) and
 208 550 nm (MODIS). Both satellite and photometer data cover the entire period of microm-
 209 eteorological and flux data, described in the next section. In the Alta Floresta, the AERONET
 210 system also has individual sensors and long-term measurements of incident shortwave
 211 solar radiation (SW_{ia}), as described in Table 1.

2.2.2 *Micrometeorological Measurements*

212
 213 The CO_2 flux data set available for this research were widely used and cited by pre-
 214 vious studies. Information regarding the systems installed in the micrometeorological tower
 215 is directly available in (Vourlitis et al., 2011). An automatic weather station (ASW) to
 216 monitor the weather in the Cláudia municipality was used between Jun2005 and Jul2008.
 217 The implanted tower follows the standard of the micrometeorological measurement tower
 218 system of the Programa LBA (L. Nagy et al., 2016; Artaxo et al., 2022). In this research,
 219 the deployed tower consists of a pyranometer, thermometer, psychrometer, anemome-
 220 ter, pluviograph, and a turbulent vortex system (*eddy covariance*). Herein, these mea-
 221 sures were used to represent the biophysical factors that affect the photosynthetic rates
 222 of forests. Micrometeorological data were measured every 30-60 s and stored by data-
 223 logger systems (CR5000) and (CR-10X), both Campbell Scientific, Inc., from which hourly
 224 averages were calculated (Vourlitis et al., 2011). The micrometeorological data set used
 225 in this work is the same used in the study prepared by Vourlitis et al. (2011), whose data
 226 are previously validated (certified). Technical details such as precision, accuracy, and cal-
 227 ibration can be found in (Vourlitis et al., 2011; Moreira et al., 2017). All direct measure-
 228 ments used are listed in Table 1.

2.2.3 *Measures of flux and concentration of CO_2*

229
 230 In Amazonia, the eddy covariance system has been widely used to measure the net
 231 CO_2 flux by the ecosystem. This system performs measurements by correlation of tur-

Table 1. List of measured variables and instrumentation used in the micrometeorological tower (at Cláudia Municipality) and AERONET station, in Alta Floresta. The *flags* [1], [2] and [3] indicate the instrumentation used in the flux tower, AERONET system and AQUA space platforms (TERRA), respectively.

Data set	Instrumentation		Attributes		
Measurements	Sensors [sites]	Models, Manuf.	Units	Symbols	Height
Inc. Solar Radiation	Pyranometer [1]	LI-200SB, LI-COR	Wm^{-2}	SW_i	40.0 m
Photosyn. Active Rad.	Pyranometer [1]	LI-190SB, LI-COR	Wm^{-2}	PAR_i	41.5 m
Atmospheric Pressure	Barometer [1]	PTB101B, VSLA	hPa	P_{air}	42.5 m
Air Temperature	Thermohygrometer [1]	CS215, RMS	$^{\circ}\text{C}$	T_{air}	41.5 m
Relative Humidity	Thermohygrometer [1]	HMP-35, VSLA	%	RH_{air}	41.5 m
Precipitation	Pluviometer [1]	GAUGE, MANUAL	mm	PRP	40.5 m
Wind Speed	Sonic Anemometer [1]	CSAT-3, CSCI	ms^{-1}	US_s	42.0 m
Wind Direction	Sonic Anemometer [1]	CSAT-3, CSCI	deg	US_d	42.0 m
CO ₂ Concentration	IRGA [1]	LI-820, LI-COR	ppm	$[\text{CO}_2]$	1-28 m
Inc. Solar Radiation	Pyranometer [2]	CM21, K&Z	Wm^{-2}	SW_{ia}	–
Photosyn. Active Rad.	PAR Energy [2]	SKYE510, SKYE	Wm^{-2}	PAR_{ia}	–
Aerosol Optical Depth	Photometer [2]	CIMEL	–	AOD_a	–
Aerosol Optical Depth	Modis-Terra [3]	MOD043K	–	AOD_m	–
Aerosol Optical Depth	Modis-Aqua [3]	MYD043K	–	AOD_m	–

232 bulent vortices from a sonic anemometer and an infrared gas chamber (Infrared Gas An-
 233 analyzer, IRGA), from which flux measurements of CO₂ (Carbon), water vapor (H₂O) and
 234 energy (sensible heat – H and latent heat – LE) are determined at high frequency, usu-
 235 ally 10Hz. The data generated and recorded by the *eddy* system, deployed in flux tow-
 236 ers, is normally adjusted by compilation software such as Alteddy 3.90 (Alterra, WUR,
 237 Netherlands), from which averages are taken every 10, 30 or 60 min (Foken, 2008). This
 238 system has been extensively described and improved in recent years (Moncrieff et al.,
 239 1997; Aubinet et al., 2001; Aubinet, 2012). The carbon flux data from these microme-
 240 teorological towers are presented, using the classical sign convention in atmospheric sci-
 241 ence. The negative flux, by convention, indicates that the displacement of the net flux
 242 of CO₂ is downward (photosynthesis), that is, the vegetation or ecosystem is absorbing
 243 carbon, while the positive flux is characterized by the release of carbon (respiration). (Goulden
 244 et al., 2004). The flux of CO₂, in particular, is a critical variable in the calculation and
 245 determination of the net exchange of CO₂ at the interface of any ecosystem, without which
 246 it is not possible to calculate the *NEE* of CO₂, according to the analysis methods de-
 247 scribed in the sections below. This procedure is possible through the coupling between
 248 LI-COR and eddy covariance systems, as illustrated in Vourlitis et al. (2002) and Vourlitis
 249 et al. (2011).

250 2.3 Methods

251 This section describes the methodological procedures used to achieve the radiative
 252 effects of aerosols on the *NEE* of CO₂ presented in section 1.1. Initially, the technical
 253 procedures used to determine the net exchange of CO₂ and to obtain the clear sky ir-
 254 radiance model, a critical step in the calculation of the relative irradiance, are presented.
 255 Next, the procedures for calculating diffuse PAR radiation and relative change *NEE* (%*NEE*),

256 used to assess ecosystem responses to fire pollution loads, are described. Procedures to
 257 assess the influence of environmental factors on *NEE* due to fires are also described.

258 **2.3.1 Method to determine the net exchange of CO₂ in the ecosystem**

259 The *NEE* is obtained from turbulent flux measurements using the eddy covariance
 260 technique taking into account the storage term $S[CO_2]$ (Aubinet, 2012; Araújo et al., 2010).
 261 Micrometeorological sensors distributed vertically along the tower are essential for the
 262 *NEE* calculations (Hollinger & Richardson, 2005), using continuous measurements of
 263 the CO₂ profile between soil and the top of the tower. Under these conditions, *NEE* can
 264 be approximated by Equation 1:

$$NEE \approx FCO_2 + S[CO_2]_p \quad (1)$$

265 where FCO_2 is called “CO₂ turbulent flux”, calculated by the *eddy* system, above
 266 the treetops (Grace et al., 1996; Burba, 2013); $S[CO_2]_p$ is the vertical profile of the con-
 267 centration of CO₂ or storage term (storage), considered a non-turbulent term, measured
 268 at discrete levels z , at thicknesses Δz_i , from near the ground surface to the point of mea-
 269 surement of covariance of turbulent vortices in the tower (Finnigan, 2006; Araújo et al.,
 270 2010; Montagnani et al., 2018). In this work, the vertical profile $S[CO_2]_p$ was stratified
 271 into 5 reference levels (1, 4, 12, 20, and 28 m). Typical diurnal conditions consist of vec-
 272 tor winds with speeds of 2.0 ms⁻¹ and $u^* = 0.20$ ms⁻¹ and predominant SSW and SE
 273 directions. Approximately 72% of the accumulated flux originates within 1 km and the
 274 representativeness of the measured CO₂ flux (footprint) is approximately 520 m (upstream
 275 of the tower), following the model proposed by (Schuepp et al., 1990). The concentra-
 276 tions [CO₂] were calculated following Aubinet et al. (2001) and Araújo et al. (2010), as
 277 reported by Vourlitis et al. (2011).

$$S[CO_2]_p = \frac{P_{air}}{RT_{air}} \int_0^z \frac{\partial[CO_2]}{\partial t} dz \quad (2)$$

278 Where: P_{air} is the atmospheric pressure (Nm⁻²), R is the molar constant of the
 279 gas (Nm mol⁻¹ K⁻¹) and T_{air} the air temperature in (°C).

280 **2.3.2 Method to determine the solar irradiance of clear sky**

281 The term clear sky was used here to designate the minimal influence of clouds and
 282 aerosols on the the solar radiation measured by the pyranometer. To estimate the amounts
 283 of direct solar radiation to the surface under minimally overcast sky conditions, the mea-
 284 surements SW_{ia} of the AERONET 2.0 system (*cloudless*) observed under clear-sky condi-
 285 tions were used, that is, $AOD \leq 0.10$ (Artaxo et al., 2022), in the absence of fire plumes.
 286 Under these conditions, we get the Equation 3; a polynomial fit of order 4, here, con-
 287 sidered representative of the entire solar spectrum (Meyers & Dale, 1983). The model
 288 $S(t)_0$ obtained was used to derive the clear-sky instants at the surface (Figure S4), be-
 289 tween 07-17h (LT), according to the formulation below:

$$SW_{ia} \{AOD \leq 0.10, \text{cloudless}\} \approx S(t)_0 = at^4 + bt^3 + ct^2 + dt + e \quad (3)$$

290 Where $S(t)_0$ is the clear-sky solar irradiance as a function of time, in Wm⁻². The
 291 parameters (a, b, c, d, e) are the coefficients of the polynomial curve and t , the time, in
 292 local hours (LT). Figure 2 shows the mean diurnal cycle of the SW_{ia} in the tower ob-
 293 servation area under different pollution conditions. The plot illustrates the sensitivity
 294 of the method applied to determine the expected irradiance levels on the canopy forest
 295 ($S(t)_0$) under varied atmospheric aerosol loads (AOD), C2, C4, and C6 curves.

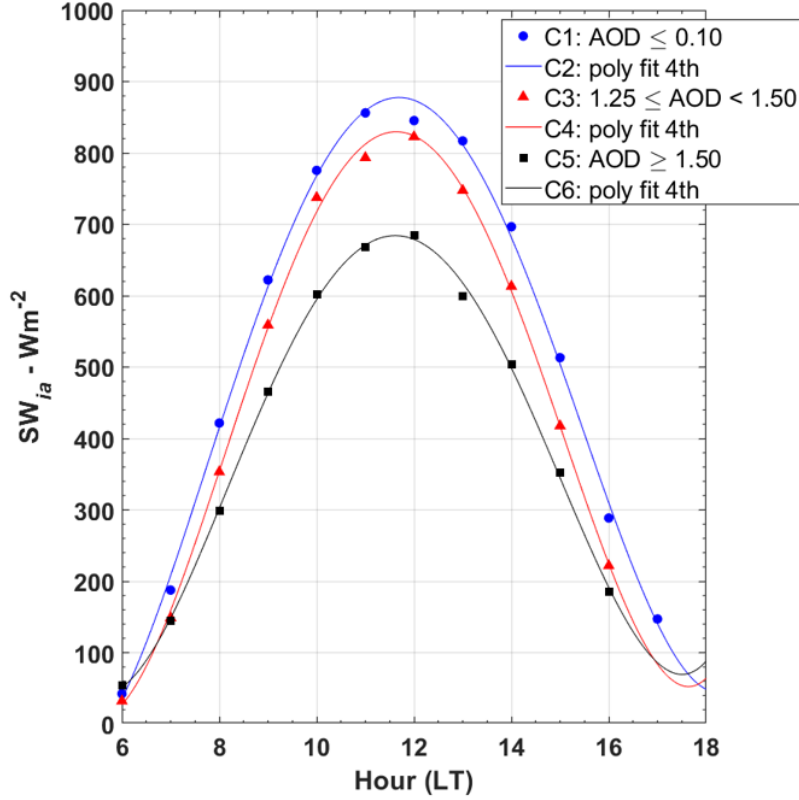


Figure 2. Incident solar irradiance under different sky conditions in Alta Floresta (1993 to 2018): clear-sky (C2 curve, $\text{AOD} \leq 0.10$) and polluted-sky (C4 curves and C6, $\text{AOD} \geq 1.25$).

296 Using the long series of measurements of AOD_a it was possible to obtain different
 297 curves $S(t)_0$ for each month of the year, taking into account the seasonal variations of
 298 the SW_{ia} given in Equation 3. Figure S4 shows the seasonal variation of the $S(t)_0$
 299 diurnal cycle throughout the year. The coefficients of the fit curves it listed in Table S1.
 300 To assess the consistency of the $S(t)_0$ model, obtained by SW_{ia} AERONET data set,
 301 we compared the outputs calculated by Equation 3 with the clear-skies solar irradiance
 302 model available by the Meteoexploration (SolarCalculator).

303 **2.3.3 Determination of relative irradiance**

304 In practical terms, the relative irradiance f expresses the relationship between in-
 305 cident solar radiation and that observed at the surface under a clear sky ($\text{AOD} < 0.10$)
 306 and “free” of clouds ($f > 1.0$). To determine it, it is necessary to calculate $S(t)_0$, given
 307 in the previous section. It is a parameter indicating the presence of clouds and/or pol-
 308 lution plumes with aerosols that scatter solar radiation, generally used in areas without
 309 direct instrumentation of cloud cover over the flux tower observation area. In these cases,
 310 f is considered a key indicator in the detection of clouds and plumes of pollution from
 311 fires in the Amazon. For this, the observed amounts of SW_{ia} on the forest canopy were
 312 normalized by the irradiance $S(t)_0$; both variables in Wm^{-2} , thus determining the quo-
 313 tient f (dimensionless parameter), according to Equation 4 below.

$$f = \frac{SW_{ia}\{AOD_a > 0.10, \text{cloudness}\}}{S_0\{AOD_a \leq 0.10, \text{cloudless}\}} \quad (4)$$

314 Where: SW_{ia} is the total incident solar irradiance measured by the pyranometer
 315 (Wm^{-2}) under any atmosphere ($AOD_a > 0.10$) and in the possibility of clouds (*cloud-*
 316 *ness*) and $S(t)_0$ is the clear sky solar irradiance (Wm^{-2}) on a flat surface perpendic-
 317 ular to the sun's rays, without the attenuating effects of the atmosphere (clouds and burned)
 318 for a given time and place, ie $AOD_a \leq 0.10$ (*cloudless*). Values off close to zero rep-
 319 resent cloudy and/or smoky-sky conditions, and values close to unity represent clear-sky
 320 conditions (Gu et al., 1999; Oliveira et al., 2007; Jing et al., 2010; G. G. Cirino et al.,
 321 2014; Gao, 2020).

322 Here, we used f as a basis for comparison to detect the joint presence of clouds and
 323 aerosols from fires over the study area, since the experimental site does not have instru-
 324 mentation for direct observation of cloud cover. Obtaining this parameter is extremely
 325 important because when using clear-sky solar radiation as a base, solar radiation mea-
 326 sured under overcast skies becomes a new metric for observing cloudiness. This variable
 327 will be compared with the *NEE* to assess the photosynthetic responses of the ecosys-
 328 tem to variations in the external environment.

329 2.3.4 Determining the clarity index

330 To determine the parameter kt (here defined as brightness index) the extraterres-
 331 trial solar irradiance S_{ext} was first calculated (depending only on orbital parameters).
 332 The index kt is a coefficient of proportionality between the measurements of direct solar
 333 radiation to the surface and S_{ext} . This index expresses the direct solar radiation trans-
 334 mitted in the atmosphere (Gu et al., 1999; G. G. Cirino et al., 2014). In a first approx-
 335 imation kt indicates the transmissivity; the degree of transparency of the atmosphere
 336 to solar radiation at a given time and place, while f is a parameter of comparison more
 337 sensitive to the presence of radiation-scattering aerosols and clouds. Here, kt and SZA
 338 were used as predictors of the diffuse component of (Gu et al., 1999; G. G. Cirino et al.,
 339 2014) radiation. For the calculation of the irradiance S_{ext} some parameters and variables
 340 are also needed such as the solar constant of the Earth (S_{ext}^t), the latitude of the loca-
 341 tion (φ), solar declination (δ), hour angle (h) and mean square distance between the Earth
 342 and the Sun (Gates, 1980). The determination of S_{ext} takes into account the angle of
 343 incidence of the solar rays and, therefore, the variations in the amounts of solar radia-
 344 tion at the surface, modulated by the SZA . Under these conditions, kt can be expressed
 345 according to Equation 5:

$$kt = \frac{SW_i\{AOD > 0.10, \text{cloudiness}\}}{S_{ext}} \quad (5)$$

346 Where SW_i is the short wave radiation measured by the pyranometer (Wm^{-2}) (Ta-
 347 ble 1) and S_{ext} the extraterrestrial solar irradiance (Wm^{-2}) estimated on a perpendic-
 348 ular surface to the sun's rays, without the attenuating effects of the atmosphere for a
 349 given time and place, expressed according to 6.

$$S_{ext} = S_{ext}^t \left(\frac{\bar{D}}{D} \right)^2 \times \cos(z) \quad (6)$$

350 In this equation S_{ext}^t is the Earth's solar constant ($\approx 1367 \text{ Wm}^{-2}$), \bar{D} is the av-
 351 erage Earth-Sun distance ($\sim 1.49 \times 10^8 \text{ km}$), D is the Earth-Sun distance on a given Ju-
 352 lian day, and $\cos(z)$ the cosine of the solar zenith angle (SZA), calculated as proposed
 353 by Bai et al. (2012). This calculated index was used to establish the diffuse solar radi-
 354 ation, as described in detail in the next section.

355

2.3.5 Determination of diffuse PAR radiation

356

357

358

359

360

361

To determine the diffuse component of the total PAR (PAR_d), we adopted the procedures of (Spitters et al., 1986) and (Reindl et al., 1990), widely used in the literature when there are no direct measurements of radiation PAR_d (Gu et al., 1999; Jing et al., 2010; Zhang et al., 2010; Bai et al., 2012). The detailed calculation can be found in the one performed by Gu et al. (1999). The estimate is performed by deriving the diffuse PAR radiation according to the formulation below (Spitters, 1986).

$$PAR_d = \left[\frac{1 + 0.3(1 - q^2)q}{1 + (1 - q^2)\cos^2(90 - z)\cos^3(z)} \right] \times PAR_i \quad (7)$$

362

363

364

365

366

367

368

369

370

Where PAR_d is the incidence of the diffuse (total) PAR radiation flux ($\mu\text{mol photon m}^{-2}\text{s}^{-1}$), in the near-infrared range, in a horizontal plane to the Earth's surface, while q is a coefficient of proportionality used to denote the ratio of the total diffuse radiation to a given amount of irradiance (SW_i) at the surface, under a given condition of the sky (Wm^{-2}). The parameter q is expressed considering ranges of variation for the index kt (Gu et al., 1999). To express the diffuse fraction of PAR radiation ($PAR(D)_f$) we use the relationship between PAR_d and PAR_i (Spitters et al., 1986). In the absence of direct measurements of diffuse solar radiation, the procedures reported by these authors are still widely used (Jing et al., 2010; G. G. Cirino et al., 2014; Moreira et al., 2017).

371

2.3.6 Determining the efficiency of light use

372

373

374

375

376

377

378

379

380

381

382

Another important parameter in this kind of study is the light use efficiency (LUE), which expresses the efficiency of light use in photosynthetic processes by the canopy. It is defined as the ratio between NEE and PAR_i . Several other procedures have been used to approximate the LUE , some use the coefficient of proportionality between the NEE and the PAR_d (Moreira et al., 2017) radiation, and others use temperature measurement directly on the leaf of the trees (LI-COR) to capture the photosynthetic response as a function of the variation in light intensity (Doughty et al., 2010). Canopy radiative transfer codes with validated physical parameterizations for different leaf types are also used (Mercado et al., 2009). Here, for practical reasons, we used the procedures applied by Jing et al. (2010) and G. G. Cirino et al. (2014), according to Equation 8, where LUE is given in percentage values.

$$LUE \approx \left(\frac{NEE}{PAR_i} \right) \quad (8)$$

383

2.3.7 Determining leaf canopy temperature

384

385

386

387

388

389

390

391

392

393

394

395

396

397

The model used to estimate the Td_f was obtained from field experiments in central Amazonia, at sites T14, T34, TN-S, and BBL4, approximately 60-70 km NW from the center of Manaus-AM. Micrometeorological and temperature measurements with thermocouples on leaves were performed on 25 and 22 samples for two different types of healthy plant species, typical of central Amazonia, distributed between 18-35 meters above the ground during the dry (July-August/2003) and rainy seasons (December 2003-February 2004), respectively. Leaf temperature measurements were performed every 15 min, between 07h and 14h (LT). Doughty et al. (2010) used alternative procedures based on pyrometer measurements to estimate leaf canopy temperature in the Tapajós National Forest (FLONA-Tapajós), in Santarém-PA, obtaining similar Td_f diurnal cycles. Here, in the absence of direct leaf temperature measurements or data from pyrgeometers operated above the canopy to measure the emission of long-wave radiation from the LW_c surface in the experimental tower (Table 1), we estimate the leaf canopy temperature (Td_f) through the formulation proposed by Tribuzy (2005). The final equation obtained

398 is expressed as a function of relative air humidity (RH_{air}) and PAR_i radiation, as shown
 399 below:

$$Td_f = [(2.48 \cdot 10^{-6}(RH_{air})^2 - 1.82 \cdot 10^{-4}(RH_{air}) - 1.83 \cdot 10^{-6}(PAR_i) + 0.0363)]^{-1} \quad (9)$$

400 **2.3.8 Determination of clear sky NEE**

401 The NEE observed on clear days ($AOD < 0.1$ and clear) was also used as a ba-
 402 sis for comparison for cloudy days and/or days with high aerosol loading. The Figure
 403 3 illustrates the behavior of the NEE under clear sky conditions ($f \approx 1.0$). The poly-
 404 nomial fit obtained is used to determine the clear sky $NEE(sza)_0$ as a function of SZA
 405 variations, between Jun2005-Jul2008. Figure 3 below illustrates the NEE variations as
 406 a function of the SZA angle. The correlation curve found is consistent with the behav-
 407 ior observed in previous studies (Gu et al., 1999; G. G. Cirino et al., 2014). The equa-
 408 tion below was used to estimate the expected NEE under the above-mentioned condi-
 409 tions.

$$NEE(sza)_0 = p_1 t^2 + p_2 t + p_3 \quad (10)$$

410 Where $NEE(sza)_0$ is the NEE typically found on clear sky days ($\mu\text{mol m}^{-2}\text{s}^{-1}$).
 411 The parameters p_1 , p_2 and p_3 the coefficients of the polynomial curve obtained, respec-
 412 tively equal to: 0.0038, -0.99 and -12 . Like f , $\%NEE$ was used here as a basis for
 413 comparison for the maximum negative values observed between Jun2005-Jul2008, assum-
 414 ing, in this analysis, the absence of water stress and nutrient deficiency in the studied
 415 period (Gu et al., 1999; Oliveira et al., 2007; Doughty et al., 2010; G. G. Cirino et al.,
 416 2014).

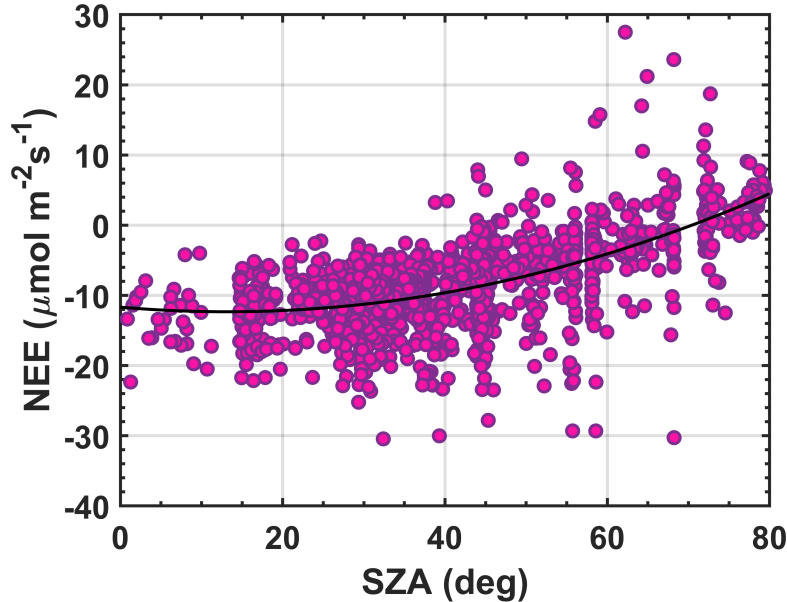


Figure 3. Correlation between NEE and SZA for clear sky conditions ($f \approx 1.0$), in the Cláudia Municipality. The black curve indicates the 2nd order polynomial fit obtained ($NEE(sza)_0$).

417 Changes in observed NEE versus NEE under clear sky conditions were used to
 418 determine the percentage effect of aerosols on NEE . The $\%NEE$ was calculated by the
 419 following relationship (Bai et al., 2012; Gu et al., 1999; Oliveira et al., 2007):

$$\%NEE = \left(\frac{NEE(sza) - NEE(sza)_0}{NEE(sza)_0} \right) \times 100 \quad (11)$$

420 To largely eliminate solar elevation angle interference in the analysis of changes in
 421 $\%NEE$ versus f , we grouped the data into SZA ranges of 20-25°. This interval was small
 422 enough to minimize the effects of solar uplift during the day and to represent changes
 423 in NEE as a function of f in response to changes in NEE flux due to aerosols and/or
 424 clouds alone. This interval also ensured sufficient sample size for statistical analyses. SZA
 425 intervals smaller than 15° significantly reduced the sample size, making it impossible to
 426 develop a robust statistical analysis (Gu et al., 1999). Values above 50 or around 0 (so-
 427 lar angles very close to the horizontal and vertical plane, respectively) were, in general,
 428 very contaminated by clouds (Gu et al., 1999; G. G. Cirino et al., 2014).

429 2.4 Data analysis procedures

430 Computational routines were developed for compilation, certification, organization,
 431 and analysis of the variables presented in Table 1. We performed fitting curves and math-
 432 ematical or statistical calculations with the packages available in (MATLAB, 2013). For
 433 data quality control, non-physical values outside acceptable levels were excluded from
 434 the database, totaling a loss of 3% of the total set of valid measurements (approximately
 435 3,600 sampled points). Data analysis consists of three fundamental steps: (1) variation
 436 of solar radiation with optical depth AOD_a analyzed as a function of irradiance f ; (2)
 437 effects of aerosols and clouds on the net exchange of CO_2 at the forest-atmosphere in-
 438 terface and, finally, (3) quantification of photosynthetic performance as a function of pol-
 439 lution loads, from which to extract if the biological critical or optimal values for envi-
 440 ronmental (exogenous) factors such as d , T_{air} , Td_f and VPD. Photosynthetic perfor-
 441 mance, in all cases, is analyzed as a function of NEE . In the end, the net percentage
 442 variation of the photosynthetic activity of the forest ($\%NEE$) is evaluated as a function
 443 of the irradiance f . The main statistical analysis procedures adopted are performed in
 444 terms of correlation graphs (3D scatter plots), that is, through the direct correlation be-
 445 tween two or three variables simultaneously, from which regression curves are determined
 446 and used to compose the representative polynomial equations of the processes under anal-
 447 ysis. The relationships found are evaluated from the Poisson correlation and tabulated
 448 in terms of basic descriptive statistical parameters such as coefficient of determination
 449 (R^2) and significance level (P_{value}) with a margin confidence of 95%. Basic descriptive
 450 statistics is also applied to the data to obtain mean values, medians, percentiles, and stan-
 451 dard deviation for the measured and estimated variables. Table 2 lists indirect variables,
 452 calculated from the dataset listed in Table 1.

453 3 Results and Discussions

454 3.1 Average daily cycle of net exchange of CO_2

455 The average daily pattern of NEE variation follows the typical pattern of tropi-
 456 cal forests in the Amazon and other tropical forests (Gu et al., 1999; Niyogi et al., 2004;
 457 von Randow et al., 2004; Araújo et al., 2010; Doughty et al., 2010). The maximum neg-
 458 ative fluxes average $-13.7 \pm 6.2 \mu\text{mol m}^{-2}\text{s}^{-1}$, often observed around 10-11h (LT), and
 459 the maximum positive $+6.8 \pm 5.8 \mu\text{mol m}^{-2}\text{s}^{-1}$, approximately constant during the night
 460 period between 19h and 05h (LT), considering the data for the entire year, between 2005-
 461 2008. These results are consistent with the processes of photosynthesis (during the day)
 462 and respiration (predominantly nocturnal), respectively. We observed a slight difference

Table 2. List of indirect (calculated) variables, symbols, and measurement units of derived quantities, according to the cited body of literature.

Indirect Measures	Symbols	Units	Literature
CO ₂ Net Exchange	<i>NEE</i>	$\mu\text{mol m}^{-2}\text{s}^{-1}$	(Vourlitis et al., 2011)
CO ₂ Flux	<i>FCO₂</i>	$\mu\text{mol m}^{-2}\text{s}^{-1}$	(Vourlitis et al., 2011)
CO ₂ Vertical Profile	<i>S[CO₂]_p</i>	ppm	(Araújo et al., 2010)
Clear Sky Solar Irradiance	<i>S(t)₀</i>	Wm^{-2}	(Author)
Solar Zenith Angle	<i>SZA</i>	Degrees	(Bai et al., 2012)
Relative Irradiance	<i>f</i>	-	(G. G. Cirino et al., 2014)
Clarity Index	<i>kt</i>	-	(Gu et al., 1999)
Extraterrestrial Solar Irrad.	<i>S_{ext}</i>	Wm^{-2}	(Gu et al., 1999)
Diffuse PAR Radiation	<i>PAR_d</i>	$\mu\text{mol phot. m}^{-2}\text{s}^{-1}$	(Gu et al., 1999)
Diffuse PAR Fraction	<i>PAR(D)_f</i>	-	(Gu et al., 1999)
Efficiency of Light Use	<i>LUE</i>	-	(Jing et al., 2010)
Leaf Canopy Temperature	<i>Td_f</i>	°C	(Tribuzy, 2005)
Clear Sky NEE Exchange	<i>NEE(sza)₀</i>	$\mu\text{mol m}^{-2}\text{s}^{-1}$	(G. G. Cirino et al., 2014)
Relative NEE Exchange	<i>%NEE</i>	%	(G. G. Cirino et al., 2014)

463 in the pattern of the daily cycle of the *NEE* flux between the wet and dry seasons (Fig-
464 ure (4)), with CO₂ absorption peaks about 10-15% lower (i.e, less negative) at both sea-
465 sons ($< 0.6 \mu\text{mol m}^{-2}\text{s}^{-1}$), when compared to the results presented by Vourlitis et al..
466 Our results also show a shift (an advance) in the peak absorption of CO₂ from the wet-
467 to-dry season, from about 12h (LT) to 10h (LT), respectively (Figure 4).

468 Seasonal variations in water availability, nutrients, radiation, temperature, VPD,
469 and pollution are counterbalanced throughout the year, producing an average seasonal
470 behavior without significant differences in *NEE*. Vourlitis et al. (2011) showed similar
471 monthly variations with more negative magnitudes during the bright hours of the day
472 in the rainy months ($-9.0 \mu\text{mol m}^{-2}\text{s}^{-1}$, between November-February) and less nega-
473 tive during the light hours in the dry months ($-7.7 \mu\text{mol m}^{-2}\text{s}^{-1}$, between May-August).
474 During night hours these values are respectively equal to $+5.4 \mu\text{mol m}^{-2}\text{s}^{-1}$ and $+7.4$
475 $\mu\text{mol m}^{-2}\text{s}^{-1}$. The general balance between these fluxes reveals 'carbon uptake' of -0.12
476 $\mu\text{mol m}^{-2}\text{s}^{-1}$ and $-0.18 \mu\text{mol m}^{-2}\text{s}^{-1}$ during the wet and dry seasons, respectively. The
477 maximum rates of photosynthesis and leaf canopy respiration, between 2005-2008, were
478 systematically observed between October-November, usually, in the first months of the
479 rainy season (Vourlitis et al., 2011).

480 3.2 The influence of aerosols on solar radiation

481 The impact of aerosol particles by fires on the SW_i flux is evaluated as a function
482 of *f*, AOD_a , *SZA*, *PAR(D)_f* and PAR_i . Figure 5 (top panel) shows the behavior of the
483 relative irradiance *f* for different levels of AOD_a pollution, in the *SZA* ranges between
484 20-50°. A close and statistically significant relationship between *f* and AOD_a is observed
485 with p-value < 0.01 and R^2 of about 0.92 (Table 3). An approximately linear relation-
486 ship is observed in which *f* decreases by about 40-60% when the AOD_a varies from 0.10
487 to 5.0. No statistically significant difference was observed between mornings and after-
488 noons in these analyses. There is only a slight increase of $\approx 5\text{-}20\%$ (on average) in the
489 value of *f* between late mornings and afternoons, attributed here to the multiple scat-

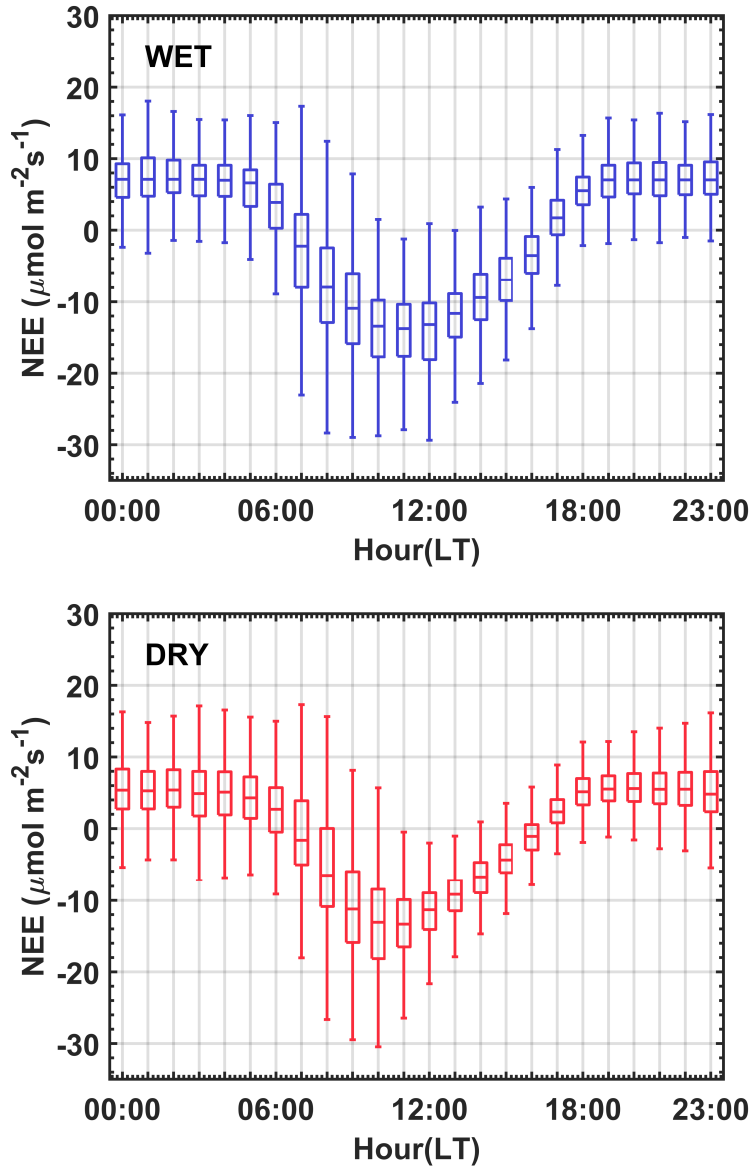


Figure 4. *NEE* average hourly cycle between June/2005 and July/2008, during the rainy (WET) and less rainy (DRY) seasons in a semideciduous forest in the Cláudia municipality, 50 km northeast of Sinop, Mato Grosso. The standard deviation is shown as vertical bars.

490 tering of solar radiation due to the formation of clouds nearby from the observation tower
 491 (Gu et al., 2001). For SZA angles between 20 and 50° , there is a strong reduction in the
 492 amounts of SW_i ($225 \pm 50 \text{ Wm}^{-2}$) associated mainly with the increase in the concen-
 493 tration of aerosols emitted by local fires or transported regionally during the burning sea-
 494 son. Oliveira et al. (2007) and G. G. Cirino et al. (2014) reported results about 2-3 times
 495 lower for 20-30% reductions in f and AOD increase from 0.1 to 0.8, in FLONA-Tapajós
 496 (Santarém-PA) and central Amazon (K4), in Manaus-AM.

497 Figure 5 (bottom panel) shows the fraction of diffuse radiation calculated as a func-
 498 tion of AOD_a , identifying important statistical relationship is also observed ($R^2 = 0.98$
 499 and 0.96) for the morning and afternoon hours (Table 3). Due to the reduction in the

500 instantaneous fluxes of SW_i an increase of about up to 85% in diffuse radiation is ob-
 501 served when the AOD_a increases from 0.10 to 5.0. These results are consistent with pre-
 502 vious studies carried out in the Brazilian Amazon (Doughty et al., 2010; G. G. Cirino
 503 et al., 2014; Rap, 2015; Moreira et al., 2017; Malavelle et al., 2019; Bian et al., 2021) and
 504 also around the world (Niyogi et al., 2004; Jing et al., 2010; Rap, 2015; Rap et al., 2018)
 505 and proves to be particularly important due to the ability of PAR_d to penetrate more
 506 efficiently into the leaf canopy contributing, under certain conditions, to a significant in-
 507 crease in carbon uptake by the ecosystem.

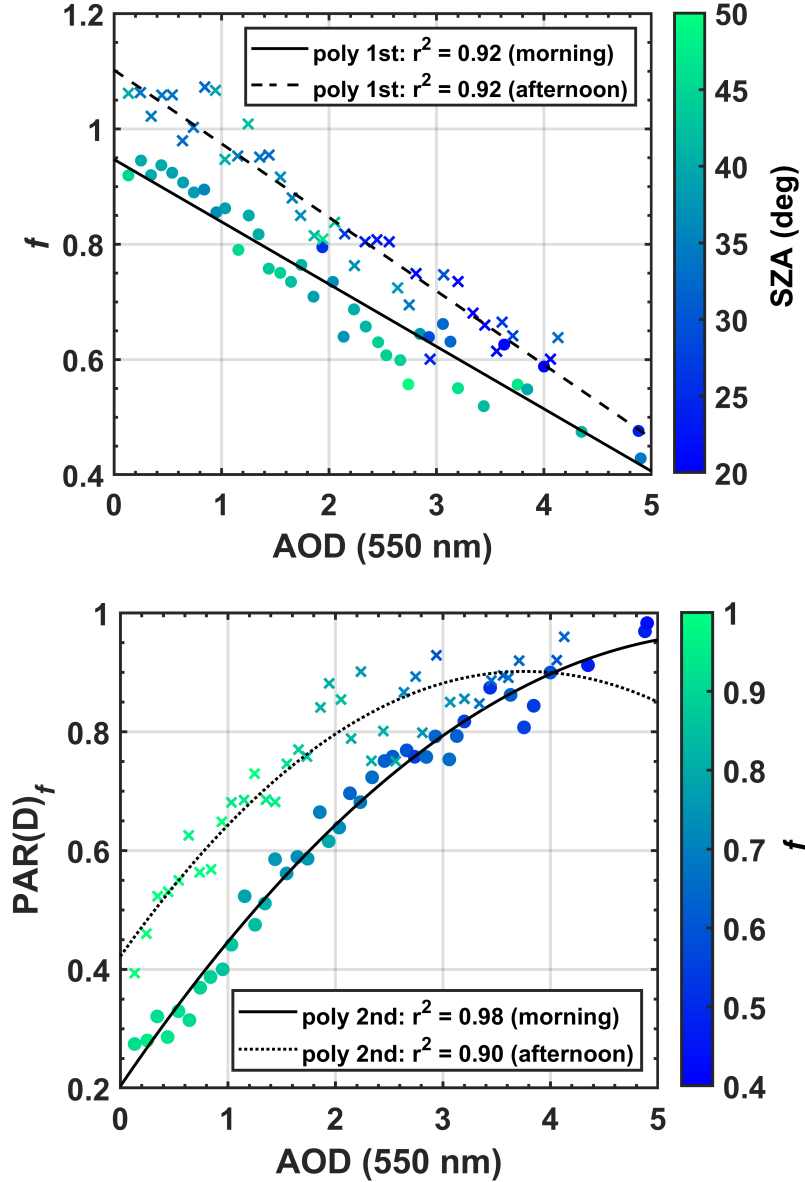


Figure 5. 3D-correlation between f and $PAR(D)_f$ with increasing AOD_a for different values SZA (top panel) and irradiance f (bottom panel) in semi-deciduous forest in the Cláudia municipality, 50 km northeast of Sinop-MT (2005-2008).

Table 3. Polynomial adjustments (Figure 5), coefficients and statistics for the morning and afternoon periods in the micrometeorological tower in Cláudia-MT (2005-2008). R^2 is the correlation coefficient, ΔSW_i is the incident shortwave radiation amount, and STD is the Standard Deviation.

Settings		Period	Coefficients			Statistics	
Polynomial Functions		Local Hours	a	b	c	R^2	ΔSW_i (STD)
f	poly fit 1st	07-12h	-0.11	0.95		0.92	-200 (± 50)
		12-17h	-0.13	1.10		0.92	-250 (± 80)
$PAR(D)_f$	poly fit 2nd	07-12h	-0.023	0.27	0.20	0.98	-97 (± 30)
		12-17h	-0.034	0.25	0.42	0.90	-118 (± 42)

508

3.3 The influence of aerosols on PAR radiation

509

510

511

512

513

514

515

516

Figure 6 shows the behavior of the radiation PAR_i and PAR_d as a function of f and SZA . For reductions of $\approx 40\%$ in f , that is, for f ranging from 1.0 to 0.6, strong reductions in radiation PAR_i ($\sim 750 \mu\text{mol m}^{-2}\text{s}^{-1}$), corresponding to a 55% increase in radiation PAR_d ($\sim 600 \mu\text{mol m}^{-2}\text{s}^{-1}$). This behavior was observed between July-November of the years 2005-2008, during selected clear-sky days. These numbers indicate a strong reduction in PAR_i as pollution levels increase and change from clear sky conditions ($AOD \leq 0.10$, $f \sim 1.0$) to aerosol smoky sky conditions of fires ($AOD \gg 0.1$, $f \ll 1.0$).

517

518

519

520

521

522

523

524

525

526

PAR_i decreased almost linearly with respect to f (Figure 6, top panel). The relationship between PAR_d radiation and f does not show a linear behavior (Figure 6, bottom panel). PAR_d values reach maximum values ($779\text{-}1080 \mu\text{mol m}^{-2}\text{s}^{-1}$) for values of f between 0.63 and 0.66 (reductions of 37 %-34%) for ranges SZA ($20\text{-}40^\circ$). As will be seen below, these values are considered critical for maximum CO_2 absorption rates (maximum-negative NEE). The 50% increase in PAR_d can be explained by aerosol dispersion during the biomass burning season (July-November), results mainly attributed to the dense layer of radiation-scattering aerosols, typical of Biomass Burning Organic Aerosols (BBOA) aerosols (Shilling et al., 2018; de Sá et al., 2019). The polynomial fits, coefficients, and inflection points are displayed in Table 4.

Table 4. Polynomial adjustments (Figure 6), coefficients, and statistics for the morning and afternoon periods in the micrometeorological tower in Cláudia-MT (2005-2008). $Cp(x_v, y_v)$ is the critical point of the fit curve, where the derivative is equal to zero.

Settings		Angles	Coefficients				Statistic	
Polynomial Functions		SZA	a	b	c	d	R^2	$Cp(x_v, y_v)$
PAR_i	poly 1st	0-20°	$+1.5 \times 10^3$	+56			0.92	
		20-40°	$+2.0 \times 10^3$	+41			0.86	
		40-60°	$+1.7 \times 10^3$	+57			0.64	
		0-60°	$+1.3 \times 10^3$	-23			0.67	
PAR_d	poly 3rd	0-20°	-2.5×10^3	$+8.4 \times 10^2$	$+2.2 \times 10^3$	-19	0.92	(0.66, 1080)
		20-40°	-1.3×10^3	-5.6×10^2	$+2.3 \times 10^3$	-56	0.66	(0.63, 846)
		40-60°	-6.4×10^2	-7.0×10^2	$+1.6 \times 10^3$	-41	0.42	(0.61, 529)
		0-60°	-2.0×10^3	$+5.8 \times 10^2$	$+1.7 \times 10^3$	-22	0.40	(0.63, 779)

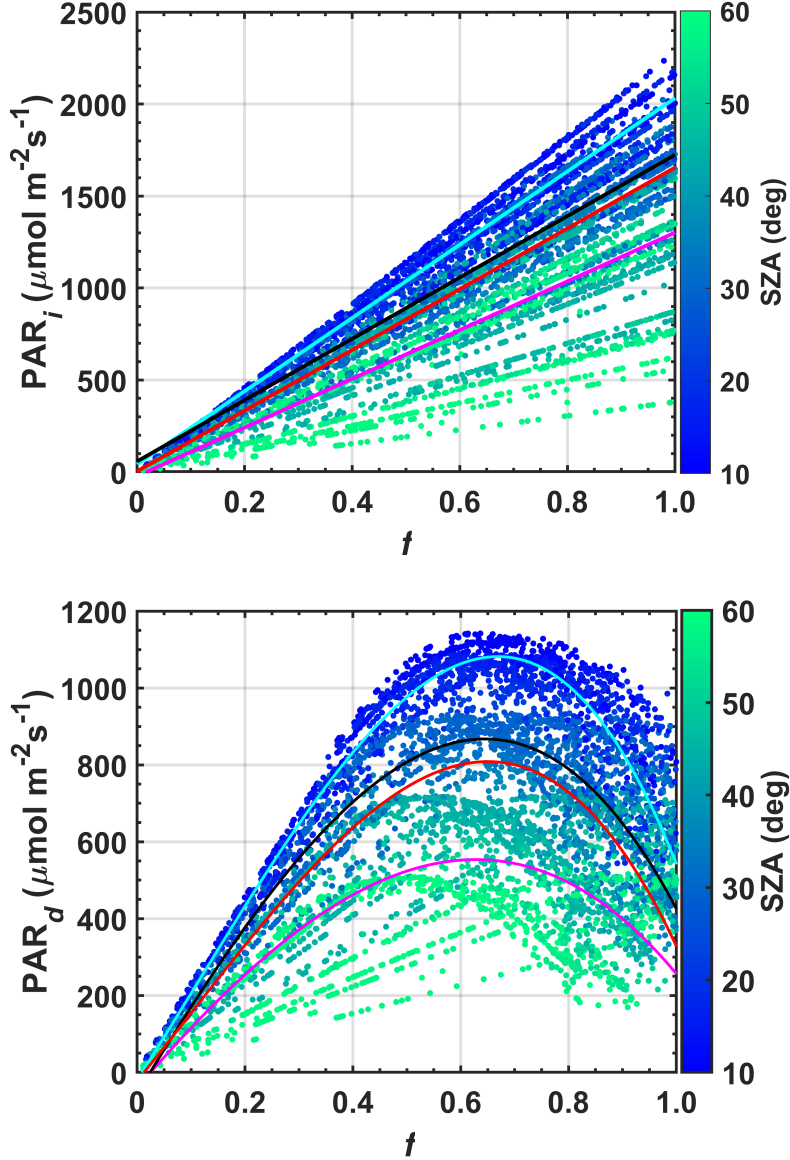


Figure 6. 3D-correlation between f , PAR_i (top panel) and PAR_d (bottom panel) for different SZA values. The blue, black, magenta and red lines are the polynomial curves adjusted to the analyzed SZA variation ranges, respectively equal to $0-20^\circ$, $20-40^\circ$, $40-60^\circ$, and $0-60^\circ$, in semi-deciduous forest in the Cláudia municipality, 50 km northeast of Sinop-MT (2005-2008).

527
528

3.4 The indirect effect of aerosols on the use of light efficiency by the forest

529
530
531
532
533
534
535

Due to the burning season, there was a well-defined monthly variation of AOD_a , as shown in the previous sections. Since fires are the main cause of changes in the physical and chemical composition of the atmosphere throughout the year (Martin, Andreae, Artaxo, et al., 2010; Martin, Andreae, Althausen, et al., 2010; Artaxo et al., 2013, 2022), statistically significant reductions were found for the SW_i flux and radiation PAR_i . This section mainly evaluates the optimal levels of PAR_i radiation, as well as the effects of changes in the efficiency of solar radiation use by the forest (LUE). The LUE , here, is

536 expressed in terms of the quotient between the fluxes NEE and PAR_i , Equation 8, as
 537 already mentioned in the section before (Sec. 2.3.5). The analyses are performed as a
 538 function of PAR_d radiation, from which the maximum efficiency of light use for the stud-
 539 ied semideciduous forest is determined.

540 Under smoky sky conditions ($AOD \gg 0.10$), carbon assimilation gradually increases
 541 with increasing total PAR radiation (PAR_i) reaching maximum saturation around 1550
 542 and 1870 $\mu\text{mol m}^{-2}\text{s}^{-1}$ in the range between 20-50° SZA , values for which the max-
 543 imum NEE (negative) occurs around $-23 \mu\text{mol m}^{-2}\text{s}^{-1}$. Under clear sky conditions,
 544 considering the same SZA range, the maximum saturation (maximum negative NEE),
 545 occurs around 2100-2300 $\mu\text{mol m}^{-2}\text{s}^{-1}$, that is, around $-18 \mu\text{mol m}^{-2}\text{s}^{-1}$ (Figure 7, top
 546 panel). To complement this analysis, the NEE flux was normalized by the radiation PAR_i
 547 and plotted against the $PAR(D)_f$ during days with high aerosol loading in the burn-
 548 ing season (Figure 7, bottom panel). Under these conditions, it is observed that the fore-
 549 est reaches maximum NEE fluxes (negative) on smoky days and not under clear sky (sunny)
 550 conditions. The results reveal that smaller amounts of energy are needed for the forest
 551 to reach maximum saturation on non-polluted days. The analyzes presented in Figure
 552 7 confirm greater photosynthetic efficiency (under smoky sky conditions) for the stud-
 553 ied semideciduous forest ecosystem, results compatible with field observations (Oliveira
 554 et al., 2007; Doughty et al., 2010; G. G. Cirino et al., 2014) and by numerical modeling
 555 in the Amazon (Rap, 2015; Moreira et al., 2017; Malavelle et al., 2019; Bian et al., 2021)
 556 and in the world (Rap et al., 2018). Due to the physicochemical nature of the BBOA
 557 and its intrinsic properties (G. Cirino et al., 2018; Adachi et al., 2020) the radiation PAR_d
 558 can strongly affect the NEE and the functioning of several other Amazon forest ecosys-
 559 tems (Rap, 2015; Rap et al., 2018; Bian et al., 2021), especially where tree species adapted
 560 to low light conditions occur, for example, in the leaf sub-canopy of Amazonian forests
 561 (Mercado et al., 2009).

562 Photosynthetic efficiency (LUE), closely linked to the canopy's ability to convert
 563 solar energy into biomass, is ~ 1 -2% for the studied forest, indicating loss or rejection
 564 of a large part of the solar energy available for photosynthesis. However, for high val-
 565 ues of PAR_d , close to 1.0, peaks of up to 3% in photosynthetic efficiency are observed.
 566 In situations where the diffuse fraction total maximum values, the values of AOD_a are
 567 on average greater than 1.0 and $f \ll 1.0$. These findings corroborate the previous an-
 568 alyzes and reinforce the presence of radiation-scattering aerosols emitted by the fires over
 569 the studied area. Although there is great uncertainty (high standard deviation) in the
 570 behavior of LUE with increasing radiation PAR_d , there is a gradual, approximately lin-
 571 ear increase in the values of LUE in the range of radiation PAR_d between 0.20-1.0. This
 572 behavior is peculiar to tall vegetation with a generally leafy canopy of tropical forests,
 573 which are more sensitive to the transfer of PAR_d radiation from the top canopy to the
 574 bole. In short stature vegetation, as in the semiarid region of northeast China (eg grasses),
 575 the LUE remains approximately constant even for high values of PAR_d generated by
 576 aerosols and clouds (Jing et al., 2010). Overall, however, the LUE is low for many veg-
 577 etation types, typically between 1-3%.

578 3.5 The net absorption of CO_2 due to aerosols from fires

579 The Equation 11 and Equation 4 allowed us to evaluate the behavior of the ratio
 580 between the % NEE and the irradiance f for intervals SZA from 0-75°. This procedure
 581 was adopted to minimize the effects of solar elevation and air temperature on the NEE
 582 flux throughout the day (Gu et al., 1999; G. G. Cirino et al., 2014). The intervals ev-
 583 ery 25° ensured the smallest possible SZA variations and the largest possible number
 584 of points within the sample space necessary for statistical analyses. For each SZA in-
 585 terval analyzed, the average % NEE was evaluated in *bins* of f equal to 0.1, calculated
 586 separately (Figure 8). The critical points and the coefficients of curves for all data (be-
 587 tween 0-75° SZA) are shown in the supplementary material (Figure S5, Table S2). On

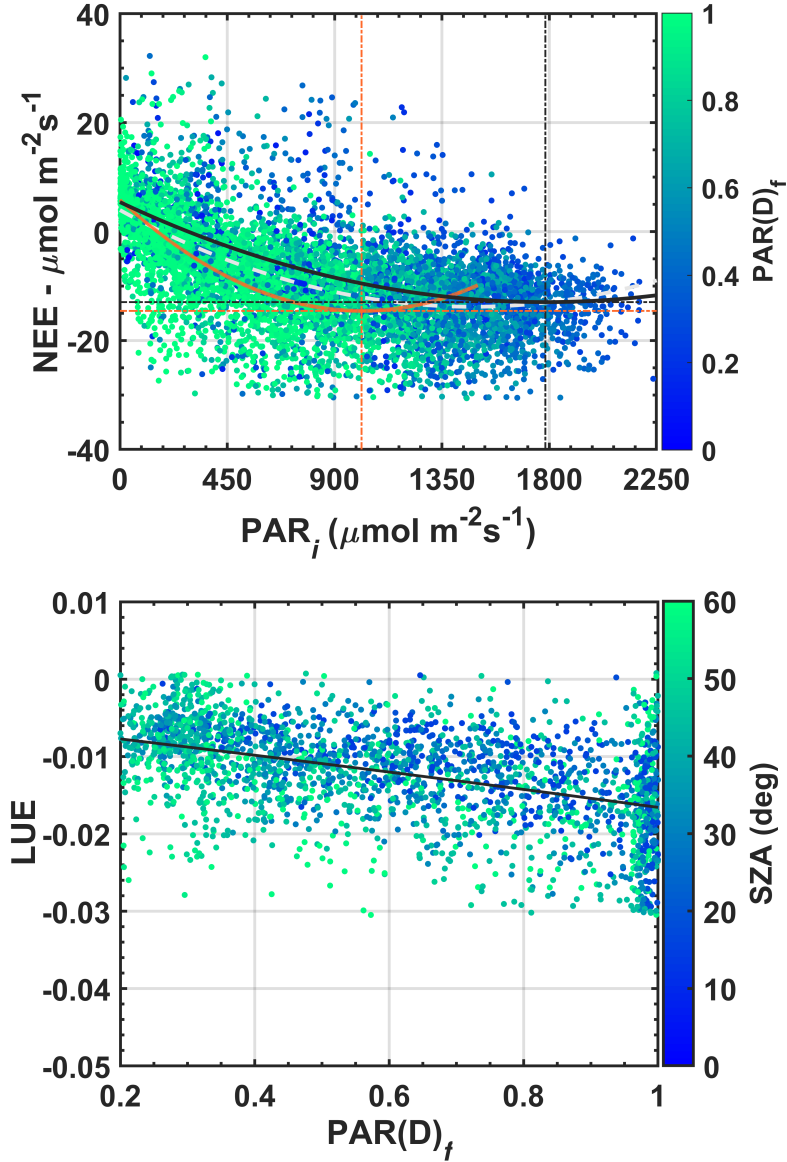


Figure 7. *NEE* as a function of radiation PAR_i for measurements between 08h and 17h LT (top panel). The bottom panel shows the *LUE* as a function of the fraction $\text{PAR}(D)_f$ ($R^2 = 0.21$, the value of $p < 0.001$) for an area of semideciduous forest located in the municipality of Cláudia- MT, 50 km north of Sinop, between Jun2005-Jul2008.

588 average, an average (absolute) increase of approximately $7.0 \mu\text{mol m}^{-2}\text{s}^{-1}$ in carbon up-
 589 take was observed relative to clear sky conditions ($NEE(sza)_0$), when f varied from 1.1-
 590 1.0 to 0.66, results for the *SZA* range between $0-75^\circ$ (Figure 8, top panel). The $7.0 \mu\text{mol}$
 591 $\text{m}^{-2}\text{s}^{-1}$ increase represents a 20-70% increase in *NEE* flux. This increase, strongly linked
 592 to the increase in aerosol concentration by fires, is mainly explained by the 50% increase
 593 in radiation $\text{PAR}(D)_f$ (approximately $450 \mu\text{mol m}^{-2}\text{s}^{-1}$ in the stream PAR_d) and 35-
 594 40% reduction in the irradiance f when the AOD_a varies from 0.10 to 5.0 (Figure 5, bot-
 595 tom panel).

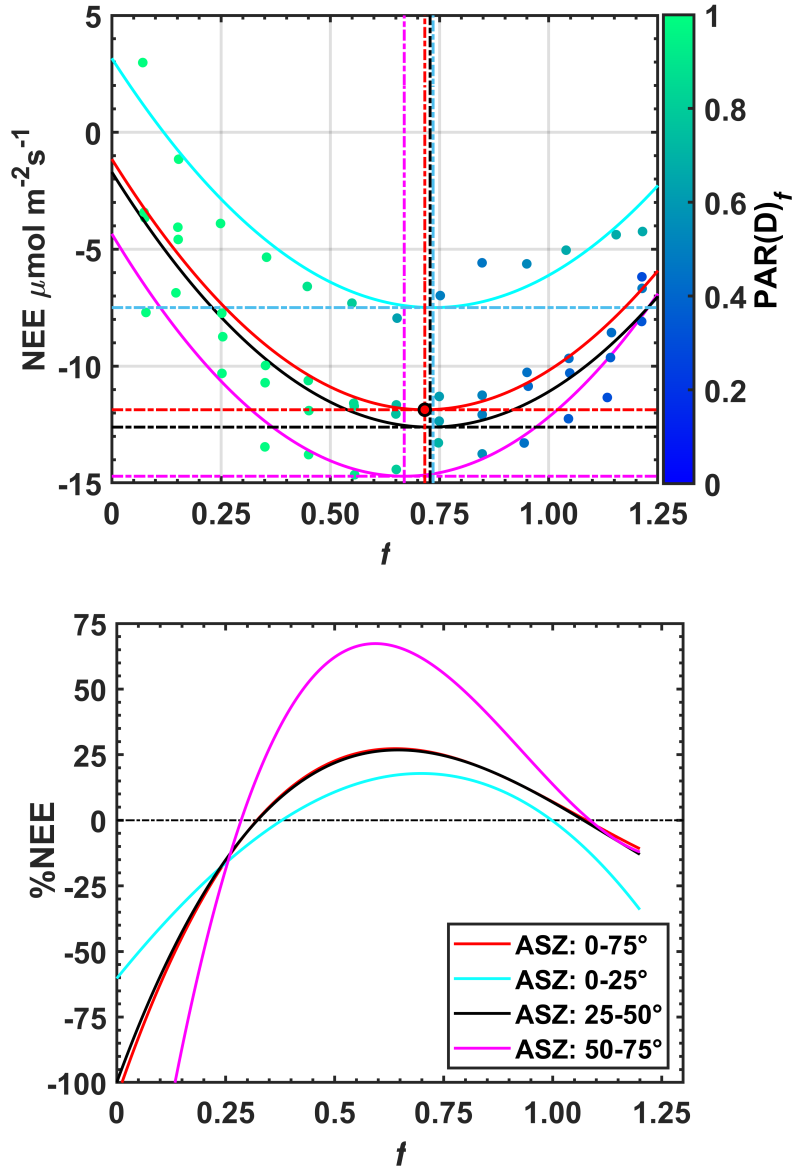


Figure 8. Variability of NEE with f for various SZA ranges in the top panel. The $\%NEE$ as a function of the irradiance f for the same SZA intervals is shown in the bottom panel. These graphs include the effects of aerosols in the experimental area of Cláudia-MT, between 2005-2008.

596 Oliveira et al. (2007) and (G. G. Cirino et al., 2014)(2014) showed a relative in-
 597 crease of about 30% for f values ranging from 1.1 to 0.80. The negative variations in f ,
 598 also indicated a high pollution load for fires at the site (AOD between 0.10-2.5) (Fig-
 599 ure 5, bottom panel) producing statistically significant reductions of up to 35% in the
 600 PAR radiation flux and a 47% increase in $\text{PAR}(D)_f$ (Figure 5, Figure 6, both bottom
 601 panel). These studies showed that the increase in carbon uptake, in the presence of aerosols
 602 and clouds, becomes smaller and similar in both locations for SZA bands < 20 . Solar
 603 radiation suffers less scattering near the zenith ($SZA \sim 10^\circ$) due to particles suspended
 604 in the atmosphere due to the narrowing of the optical path, reducing the effects of dif-
 605 fuse radiation on the photosynthetic process. These results, in particular, are generally

repeated for the studied semi-deciduous forest of Mato Grosso, but a strong increase of 70% in %*NEE* is observed for lower *SZA* ranges (between 50-75%), in the early hours of the day, between 8-10h (LT), while in the Jaru Biological Reserve (JBR) the biggest increases are concentrated in the *SZA* ranges between 10-35°, close to midday, or in the morning-afternoon (Oliveira et al., 2007). At K34, in Manaus, the maximum absorptions and the maximum %*NEE* occur do not exceed 20% and the effects of aerosols and clouds operate together. The individual radiative influences of clouds and aerosols are difficult to quantify because satellite AOD observations have a low temporal resolution. Similar results were observed by Doughty et al. (2010) in FLONA-Tapajós, central Amazon. In general, higher standard deviations are found in regions most heavily impacted by aerosols, such as Ji-Paraná (RO) and Altafloresta (MT). Because aerosol concentrations are relatively lower in FLONA-Tapajós (PA) and Manaus (AM), the standard deviations are lower. Table 5 lists the coefficients of the adjustments found between %*NEE* and *f* for each of the considered ranges *SZA*, as well as the critical points (herein called biological optimum) for the irradiance values *f* and *NEE* flux ($\mu\text{mol m}^{-2}\text{s}^{-1}$).

These results are considered relevant, as a large part of the Amazon area is frequently impacted by the presence of aerosols in small amounts (low AOD), similar to those observed in the north of the Amazon basin, in Manaus-AM. In other regions, however, increases in the absorption of CO₂ are significant and can have major impacts on the carbon budget of the Amazon forest (as in the acro region of deforestation). Over dense forest ecosystems of central Amazonia, CO₂ absorption peaks are often observed at larger and narrower intervals, generally between 1.1 to 0.80; particularly observed value for dense forest ecosystems (Gu et al., 1999; Yamasoe et al., 2006; Oliveira et al., 2007; Doughty et al., 2010), and quite different from what is observed in grasslands and temperate forest regions of the world, where the maximum *NEE* (negative) is generally found in the range *f* between 1.0-0.5 (5-10 $\mu\text{mol m}^{-2}\text{s}^{-1}$) (Gu et al., 1999; Niyogi et al., 2004; Jing et al., 2010; Zhang et al., 2010).

The mechanisms used to explain the computation of the %*NEE* with the irradiance *f* is complex and also influenced by the dynamics of the Planetary Boundary Layer (PBL) throughout the day, including transport of regionally transported and locally emitted burning emissions. For the semideciduous forests studied here, an accumulation of aerosols from fires during the night hours (19h to 06h, LT) may be associated with greater stability in the PBL during the fire season (lower values in wind speed, reduction in convection and boundary layer narrowing). These factors can increase the concentration of aerosols (AOD_a) during the night hours, with important effects on the CO₂ absorption capacity (%*NEE*) observed in the early hours of the day (*SZA* values between 50-75°). Given the dynamics of particulate transport (aerosol advection) from other regions to the experimental study area, higher CO₂ absorption capacities (%*NEE*) can be found in other types of forest ecosystems in the Amazon basin. Future studies may elucidate the dynamic effects of PBL on the photosynthetic capacity of forests in the Amazon Basin, like studies carried out in other forests around the world; in Wisconsin, EUA (Helliker & Ehleringer, 2000; Yakir, 2003); in Beijing, China (X. Wang et al., 2021; Z. Wang et al., 2022). Field experiments focused on radiative transfer from the leaf canopy, that is, on the vertical distribution of PAR_{*f*} radiation from the top to the top of the canopy, inside the forests, will improve the current understanding of the individual effects of aerosols and clouds on %*NEE* due to the cooling caused in *Td_f* and VPD, considered important biophysical variables essential for forest photosynthesis (ecosystem functioning).

3.6 Effects of fires on biophysical variables

Important direct interference of aerosols on environmental variables that consequently affect the photosynthetic dynamics of plants is observed in Figure 9 (von Randow et al., 2004; G. G. Cirino et al., 2014). The attenuating effect of incident solar irradiance due to the presence of aerosols triggers statistically significant reductions in air temperature

Table 5. Polynomial adjustments (Figure 8), coefficients, and statistics for the periods between 07-17h (LT) in the micrometeorological tower 50 km from Sinop-MT, in the municipality of Cláudia, between 2005-2008.

Settings	Angles	Coefficients				Statistic	
Poly fit 2nd	ASZ	<i>a</i>	<i>b</i>	<i>c</i>	<i>d</i>	R^2	$Cp(x_v, y_v)$
NEE	0-25°	+23	-31	-4.3		0.88	(0.74, -07.50)
	25-50°	+21	-30	-1.7		0.95	(0.73, -12.61)
	50-75°	+20	-29	+3.1		0.88	(0.67, -14.71)
	0-75°	+21	-30	-1.1		0.97	(0.72, -11.90)
Poly fit 3rd	ASZ	<i>a</i>	<i>b</i>	<i>c</i>	<i>d</i>	R^2	$Cp(x_v, y_v)$
%NEE	0-25°	-38	-1.1×10^2	$+2.1 \times 10^2$	-60	0.88	(0.70, 20.06)
	25-50°	$+1.5 \times 10^2$	-4.9×10^2	$+4.5 \times 10^2$	-1.0×10^2	0.97	(0.68, 26.68)
	50-75°	$+5.4 \times 10^2$	-1.5×10^3	$+1.2 \times 10^3$	-2.4×10^2	0.97	(0.58, 56.77)
	0-75°	$+1.7 \times 10^2$	-5.4×10^2	$+4.9 \times 10^2$	-1.1×10^2	0.98	(0.66, 27.05)

658 near the forest canopy. Several mechanisms have been used to explain the increase in
659 photosynthetic capacity by the canopy due to changes in the biophysical properties of
660 the forest, among them, the general trend of decreasing VPD (Vapour-Pressure Deficit)
661 under cloudy or smoky skies (Min, 2005; Yuan et al., 2019) and cooldowns of up to 3–4
662 °C (Koren et al., 2014; Bai et al., 2012). In this present research, reductions in temper-
663 ature and VPD, intrinsically linked to relative humidity, are also observed (Figure 9).
664 In the semi-deciduous forest of Mato Grosso, the impact of aerosols produced, respec-
665 tively, a cooling of 3 °C and 2.5 °C in Td_f and T_{ar} when f jumped from 1.1-1.10 to 0.66
666 (Figure 9, on top panel and middle panel). These results are similar to the results found
667 by (Davidi et al., 2009). The effects of these coolings, especially in Td_f , could not be heated
668 in isolation, but they can exert a large influence on the photosynthesis of the forest (Doughty
669 et al., 2010), inducing positive variations in the flux %NEE, considering the same vari-
670 ations pointed at f (Doughty et al., 2010).

671 Figure 9 (bottom panel) shows the relationship between the VPD and the irradiance
672 f (this time, between SZA angles of 0-60°). For Freedman et al. (1998), the increase
673 in relative humidity due to cooling induced by clouds and/or aerosols (Altaratz et al.,
674 2008) can increase photosynthesis, as this increase naturally induces the opening of stom-
675 ata of leaves (Collatz et al., 1991; Jing et al., 2010). In many forest locations, the reduc-
676 tion in f produces a decrease in VPD of around 35% during the dry season. These re-
677 ductions, strongly influenced by the cooling of the air, are also closely linked with the
678 cooling of the forest canopy and the increase in the absorption capacity of CO_2 (%NEE)
679 (Doughty et al., 2010). For cloudy and/or polluted sky conditions, generally decreasing
680 VPD behavior can influence stomata opening and intensify photosynthesis (Jing et al.,
681 2010). Studies focused on the impacts of fires on the flux of water to the atmosphere de-
682 serve attention and expansion in this sense. the results can help to understand the role
683 of forests in maintaining rainfall and its effects on the hydrological cycle (studies not yet
684 carried out for most biomes in the Amazon).

685 The results presented in Figure 9, viewed as a function of the frequency distribu-
686 tion of the clarity index kt , indicate that the current patterns of aerosol loading on the
687 studied semideciduous forest ecosystem exceed the maximum limit for the which dense
688 upland forests of central Amazônia reach the maximum amounts of carbon uptake (re-

sults not shown) (Oliveira et al., 2007; G. G. Cirino et al., 2014; Doughty et al., 2010). This scientific finding, in particular, apparently reveals greater tolerance (resilience) of semideciduous forests to aerosol loads by fires, considering the persistent and high loads of aerosols by fires in the Mato Grosso region over the last 30 years.

Unlike what was found here, the forests of central Amazonia, in Manaus-AM (K34), FLONA-Tapajós (K83), Santarém-PA and Ji-Paraná (RO) seem to be less tolerant to the attenuations of sunlight (induced by clouds and aerosols), required for the photosynthesis process. In the studied semideciduous forest, the distribution of kt is close to 0.66 for $AOD_a \gg 0.10$ Table 5. This value is 15-20% lower than the f values found in central Amazonia, when the NEE reaches maximum negative values during the burning season ($kt \sim 0.80$). This is the threshold value at which maximum carbon absorption is observed due to cloudiness and/or aerosol load in the JBR in the Ji-Paraná JBR (south of the Amazon basin) as well as in the Cuieiras reserve at K34, in Manaus-AM. These analyzes and comparisons are relevant because higher (lower) amounts of aerosols and clouds in the Amazon region can cause certain types of forests to absorb even higher (lower) amounts of carbon throughout the day, depending on fluctuations in light levels due to aerosols and clouds along the leaf canopy or in the regions between the ground and top of forests (Gu et al., 1999; G. G. Cirino et al., 2014). The kt frequency distribution patterns and their impacts on photosynthesis remain unknown for many other forest types in the Amazon and around the world. The results reported here for semideciduous forests in northern Mato Grosso are also consistent with calculations by Gu et al. (1999), for temperate forests in Canada, where negative maximums in NEE flux occur for ranges kt between 0.55– 0.60.

The interannual variability of the relationship between the observed AOD_a , fire counts and NEE could not be analyzed, mainly due to the lack of a long time series of NEE flux data in the region. In the central Amazon, significant variability was observed from year to year. Higher % NEE were often found on days with high fire counts. However, water stress and nutrient availability also play an important role in the carbon uptake capacity (Gatti et al., 2014; Hofhansl et al., 2016; Gatti et al., 2021; Malhi et al., 2021). Joint modifications in these variables make it extremely difficult to quantify the individual effects of aerosols and clouds on the NEE . Field experiments taking measurements of all these aspects will yield studies with more robust and comprehensive conclusions on the ecosystem responses of Amazonian forests to external environmental disturbances such as fires.

4 Conclusion

4.1 Challenges met

The aerosol optical depth derived from the AERONET system proved to be a satisfactory key variable in the elaboration of the clear sky solar irradiance model used to determine the relative irradiance f . The conceived model can be directed to other regions of the Amazon as long as they are within the same latitude range, where there are no SW_i measurements. In this study, it was possible to separate the radiative effects of aerosols from the effects produced by clouds, combining the measurements of incident solar radiation from the AERONET system with the AOD_a measurements.

The parameter f , allowed us to satisfactorily evaluate the radiative effects of aerosols from fires on the net absorption of carbon by the studied semideciduous forest ecosystem, absorption here represented by the NEE flux. The radiative impacts on the radiation fluxes PAR_i and PAR_d , allowed us to evaluate the impairment of the efficiency of light use by the forest (LUE), which increased by ~ 1 -3% under polluted conditions (AOD_a). The changes in incident solar radiation and CO_2 flux (NEE) could be attributed to the

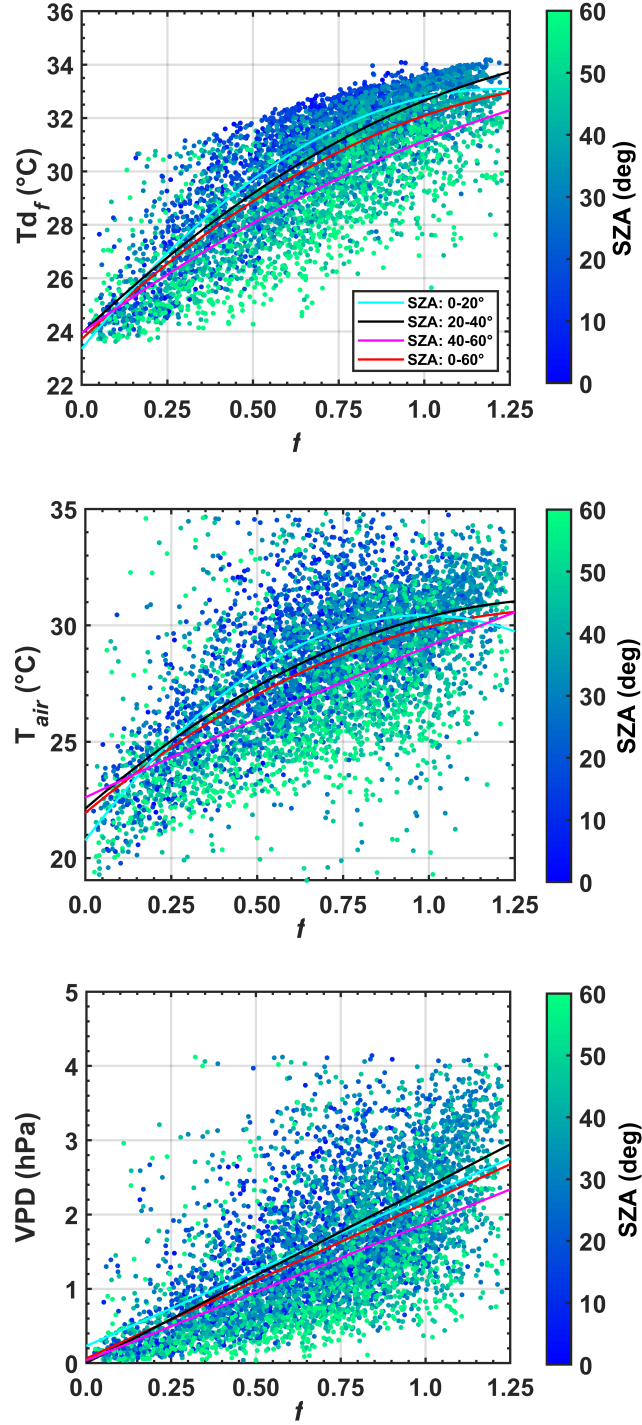


Figure 9. Correlation between the relative irradiance f with Td_f (top panel), T_{air} (middle panel) and VPD (bottom panel), values calculated for SZA between 0 and 60. The air temperature was measured at 42 m above the ground, in the micrometeorological tower located in the municipality of Cláudia, 50 km from Sinop-MT, using the parameterization given in [Tribuzy \(2005\)](#), between 2003-2004.

738 combined effects of aerosols emitted locally, regionally, or transported from more distant
739 regions, considering the applied methods.

740 In the studied semideciduous forest ecosystem, the net carbon flux (NEE) increased
741 from 20-70% when the optical depth varied from 0.1 to 5.0 (on average). This effect was
742 attributed to an average reduction of up to 40% in the amount of total PAR radiation
743 and also to an increase of up to 50% in the diffuse fraction of radiation ($PAR(D)_f$). This
744 increase in CO_2 absorption capacity by the ecosystem is closely linked to the floristic com-
745 position of the understory and certain types of forest species adapted to low light con-
746 ditions, which consists of more efficient vegetation in capturing diffused light. during the
747 photosynthesis process. The results show higher photosynthetic efficiency under smoky
748 sky conditions; loaded with particles scattering solar radiation due to fires, but also re-
749 veal the maximum limit in the PAR radiation cuts required for the photosynthesis pro-
750 cess. Relative irradiances f less than 0.66, on average, indicate the critical point at which
751 forest photosynthetic rates undergo drastic reductions. Irradiance values $f \sim$ of 0.22 in-
752 dicate 100% interruption in the photosynthetic process.

753 Due to the increase in the concentration of aerosol particles from fires in the re-
754 gion, statistically, significant changes were also observed in meteorological (biophysical)
755 variables such as leaf canopy temperature and VPD. Scientific findings reveal a strong
756 influence of fire aerosols on these variables, with potentially important effects on pho-
757 tosynthesis and carbon absorption. The 3 and 5 °C reductions in leaf canopy and air tem-
758 perature are strongly associated with a 40% reduction in f and a \sim 2.0 mb reduction
759 in VPD values which induce opening stomata and contribute to the observed increase
760 of 20-70% in the CO_2 absorption capacity of the forest ($\%NEE$). The individual influ-
761 ences or contributions of the VPD, T_{air} and Td_f to the ecosystem's net balance of CO_2 ,
762 however, could not be directly quantified in this research. Indirect correlations, however,
763 reveal statistically significant effects between the mentioned biophysical variables and
764 the observed changes in the NEE flux during the exposure of forests to fire and high
765 values of AOD_a (greater than 1.25, on average).

766 4.2 Suggestions for future work

767 A more comprehensive regional study of the effects mentioned here, based on other
768 vegetation types and biomes, using vegetation maps, remote sensing estimates, meteo-
769 rological data, and numerical modeling, will help to better understand how the climate
770 and ecosystem function in the Amazon are affected. affected by natural and anthropic
771 environmental factors. The reductions in the NEE flux and, therefore, the reduction of
772 the photosynthetic capacity of the plants due to the excessive increase in the concentra-
773 tion of BBOA aerosols and drastic reductions in the fluxes of solar radiation ($f \leq 0.22$)
774 due to the fires in the region, constitutes an effect of notable relevance for carbon cy-
775 cling in semi-deciduous forest environments in the Amazon and, therefore, an important
776 contribution to a better understanding of this cycle in the region and the world.

777 Open Research Section

778 This section provides free access to data repositories that support the conclusions.
779 Turbulent covariance data and Automatic Weather Systems, as well as selected formu-
780 las, will be available shortly on the Ameriflux website (<https://ameriflux.lbl.gov>) accord-
781 ing to Vourlitis et al. (2011): “Temporal patterns of net CO_2 exchange for a semidecid-
782 uous tropical forest in the southern Amazon Basin”. Alternatively, we provide the data
783 from this survey available through the Mendeley Data platform (<https://data.mendeley.com>),
784 where we will make upgrades and possible corrections. Citation: Cirino, Glauber; Vourli-
785 tis, George; Silva, Simone; Palácios, Rafael (2022), “Brazil-FluxMet-Stf”, Mendeley Data,
786 v1 DOI: [10.17632/m5h5fw872g.1](https://doi.org/10.17632/m5h5fw872g.1). Secondary data is already in the public domain. We
787 have listed the links to these data in the Supporting Information (Table S3).

Acknowledgments

We want to thank The National Science Foundation, National Council for Scientific and Technological Development (CNPq), and Foundation for Research Support of the State of Mato Grosso (FAPEMAT), California State University, San Marcos (CSUSM), the Federal University of Mato Grosso (UFMT) and the Union of Lumberjacks of Northern Mato Grosso (SINDUSMAD) by the funding support provided. Additional funding was provided by the CNPq Universal, project 422894/2021-4, and the Pará State Research Support Foundation (FAPESPA), grant 2022/45107. Our special thanks to Professor Dr. José de Souza Nogueira (*in memoriam*) who worked with other collaborators to generate and obtain the micrometeorological data from the measurement tower used in this research.

References

- Ackerly, D. D., Thomas, W. M. W., Ferreira, C. A. C. I. D., & Pirani, J. R. (1989). The forest-cerrado transition zone in southern Amazonia: results of the 1985 project flora amazonica expedition to Mato Grosso. , *41*(2), 113–128.
- Adachi, K., Oshima, N., Gong, Z., de Sá, S., Bateman, A. P., Martin, S. T., ... Buseck, P. R. (2020). Mixing states of Amazon basin aerosol particles transported over long distances using transmission electron microscopy. *Atmospheric Chemistry and Physics*, *20*(20), 11923–11939. Retrieved from <https://acp.copernicus.org/articles/20/11923/2020/> doi: 10.5194/acp-20-11923-2020
- Alencar, A. A. C., Arruda, V. L. S., Silva, W. V. d., Conciani, D. E., Costa, D. P., Crusco, N., ... Vélaz-Martin, E. (2022). Long-term landsat-based monthly burned area dataset for the brazilian biomes using deep learning. *Remote Sensing*, *14*(11). Retrieved from <https://www.mdpi.com/2072-4292/14/11/2510> doi: 10.3390/rs14112510
- Altaratz, O., Koren, I., & Reisin, T. (2008). Humidity impact on the aerosol effect in warm cumulus clouds. *Geophysical Research Letters*, *35*(17), 1–5. doi: 10.1029/2008GL034178
- Amorim Neto, A. d. C., Satyamurty, P., & Correia, F. W. (2015). Some observed characteristics of frontal systems in the amazon basin. *Meteorological Applications*, *22*(3), 617–635. Retrieved from <https://rmets.onlinelibrary.wiley.com/doi/abs/10.1002/met.1497> doi: <https://doi.org/10.1002/met.1497>
- Aragão, L. E., Anderson, L. O., Fonseca, M. G., Rosan, T. M., Vedovato, L. B., Wagner, F. H., ... Saatchi, S. (2018). 21st Century drought-related fires counteract the decline of Amazon deforestation carbon emissions. *Nature Communications*, *9*(1), 1–12. Retrieved from <http://dx.doi.org/10.1038/s41467-017-02771-y> doi: 10.1038/s41467-017-02771-y
- Araújo, A. C., Dolman, A. J., Waterloo, M. J., Gash, J. H., Kruijt, B., Zanchi, F. B., ... Backer, J. (2010). The spatial variability of CO₂ storage and the interpretation of eddy covariance fluxes in central Amazonia. *Agricultural and Forest Meteorology*, *150*(2), 226–237. doi: 10.1016/j.agrformet.2009.11.005
- Artaxo, P., Mohr, C., & Pöschl, U. (2022). Tropical and Boreal Forest – Atmosphere Interactions : A Review. , *74*, 24–163. doi: 10.16993/tellusb.34
- Artaxo, P., Rizzo, L. V., Brito, J. F., Barbosa, H. M., Arana, A., Sena, E. T., ... Andreae, M. O. (2013). Atmospheric aerosols in Amazonia and land use change: From natural biogenic to biomass burning conditions. *Faraday Discussions*, *165*(February 2014), 203–235. doi: 10.1039/c3fd00052d
- Aubinet, M. (2012). *Eddy Covariance*. doi: 10.1007/978-94-007-2351-1
- Aubinet, M., Chermanne, B., Vandenhaute, M., Longdoz, B., Yernaux, M., & Laitat, E. (2001). Long term carbon dioxide exchange above a mixed forest in the Belgian Ardennes. *Agricultural and Forest Meteorology*, *108*(4), 293–315. doi: 10.1016/S0168-1923(01)00244-1

- 841 Avitabile, V., Herold, M., Heuvelink, G. B., Lewis, S. L., Phillips, O. L., Asner,
842 G. P., ... Willcock, S. (2016). An integrated pan-tropical biomass map using
843 multiple reference datasets. *Global Change Biology*, *22*(4), 1406–1420. doi:
844 10.1111/gcb.13139
- 845 Bai, Y., Wang, J., Zhang, B., Zhang, Z., & Liang, J. (2012). Comparing the im-
846 pact of cloudiness on carbon dioxide exchange in a grassland and a maize
847 cropland in northwestern China. *Ecological Research*, *27*(3), 615–623. doi:
848 10.1007/s11284-012-0930-z
- 849 Balch, J. K., Brando, P. M., Nepstad, D. C., Coe, M. T., Silvério, D., Massad, T. J.,
850 ... Carvalho, K. S. (2015). The Susceptibility of Southeastern Amazon Forests
851 to Fire: Insights from a Large-Scale Burn Experiment. *BioScience*, *65*(9),
852 893–905. doi: 10.1093/biosci/biv106
- 853 Beer, C., Reichstein, M., Tomelleri, E., Ciais, P., Jung, M., Carvalhais, N., ...
854 Papale, D. (2010). Terrestrial gross carbon dioxide uptake: Global dis-
855 tribution and covariation with climate. *Science*, *329*(5993), 834–838. doi:
856 10.1126/science.1184984
- 857 Bian, H., Lee, E., Koster, R. D., Barahona, D., Chin, M., Colarco, P. R., ... Zeng,
858 F. (2021). The response of the Amazon ecosystem to the photosynthetically
859 active radiation fields: Integrating impacts of biomass burning aerosol and
860 clouds in the NASA GEOS Earth system model. *Atmospheric Chemistry and
861 Physics*, *21*(18), 14177–14197. doi: 10.5194/acp-21-14177-2021
- 862 Booth, B. B., Jones, C. D., Collins, M., Totterdell, I. J., Cox, P. M., Sitch, S.,
863 ... Lloyd, J. (2012). High sensitivity of future global warming to land
864 carbon cycle processes. *Environmental Research Letters*, *7*(2). doi:
865 10.1088/1748-9326/7/2/024002
- 866 Braghieri, Kerches Renato, Akemi Yamasoe, M., Manuel Évora do Rosário,
867 N., Ribeiro Da Rocha, H., De Souza Nogueira, J., & Carioca de Araújo,
868 A. (2020). Characterization of the radiative impact of aerosols on CO₂
869 and energy fluxes in the Amazon deforestation arch using artificial neu-
870 ral networks. *Atmospheric Chemistry and Physics*, *20*(6), 3439–3458. doi:
871 10.5194/acp-20-3439-2020
- 872 Brienen, R. J., Phillips, O. L., Feldpausch, T. R., Gloor, E., Baker, T. R., Lloyd,
873 J., ... Zagt, R. J. (2015). Long-term decline of the Amazon carbon sink.
874 *Nature*, *519*(7543), 344–348. Retrieved from [http://dx.doi.org/10.1038/
875 nature14283](http://dx.doi.org/10.1038/nature14283) doi: 10.1038/nature14283
- 876 Burba, G. (2013). *Eddy covariance method for scientific, industrial, agricultural and
877 regulatory applications: A field book on measuring ecosystem gas exchange and
878 areal emission rates*. doi: 10.13140/RG.2.1.4247.8561
- 879 Carswell, F. E., Costa, A. L., Palheta, M., Malhi, Y., Meir, P., Costa, J. d. P. R.,
880 ... Grace, J. (2002). Seasonality in co₂ and h₂o flux at an eastern amaz-
881 onian rain forest. *Journal of Geophysical Research: Atmospheres*, *107*(D20),
882 LBA 43-1-LBA 43-16. Retrieved from [https://agupubs.onlinelibrary
883 .wiley.com/doi/abs/10.1029/2000JD000284](https://agupubs.onlinelibrary.wiley.com/doi/abs/10.1029/2000JD000284) doi: [https://doi.org/10.1029/
884 2000JD000284](https://doi.org/10.1029/2000JD000284)
- 885 Cirino, G., Brito, J., Barbosa, H. M., Rizzo, L. V., Tunved, P., de Sá, S. S., ...
886 Artaxo, P. (2018). Observations of Manaus urban plume evolution and interac-
887 tion with biogenic emissions in GoAmazon 2014/5. *Atmospheric Environment*,
888 *191*(August), 513–524. doi: 10.1016/j.atmosenv.2018.08.031
- 889 Cirino, G. G., Souza, R. A., Adams, D. K., & Artaxo, P. (2014). The effect of
890 atmospheric aerosol particles and clouds on net ecosystem exchange in the
891 Amazon. *Atmospheric Chemistry and Physics*, *14*(13), 6523–6543. doi:
892 10.5194/acp-14-6523-2014
- 893 Collatz, G. J., Ball, J. T., Grivet, C., & Berry, J. A. (1991). Physiological and
894 environmental regulation of stomatal conductance, photosynthesis and tran-
895 spiration: a model that includes a laminar boundary layer. *Agricultural and*

- 896 *Forest Meteorology*, 54(2-4), 107–136. doi: 10.1016/0168-1923(91)90002-8
- 897 Davidi, A., Koren, I., & Remer, L. (2009). Direct measurements of the effect of
898 biomass burning over the Amazon on the atmospheric temperature profile. *At-*
899 *mospheric Chemistry and Physics*, 9(21), 8211–8221. doi: 10.5194/acp-9-8211
900 -2009
- 901 de Magalhães, N., Evangelista, H., Condom, T., Rabatel, A., & Ginot, P. (2019).
902 Amazonian Biomass Burning Enhances Tropical Andean Glaciers Melting.
903 *Scientific Reports*, 9(1), 1–12. doi: 10.1038/s41598-019-53284-1
- 904 de Sá, S. S., Rizzo, L. V., Palm, B. B., Campuzano-Jost, P., Day, D. A., Yee,
905 L. D., ... Martin, S. T. (2019). Contributions of biomass-burning, ur-
906 ban, and biogenic emissions to the concentrations and light-absorbing
907 properties of particulate matter in central amazonia during the dry sea-
908 son. *Atmospheric Chemistry and Physics*, 19(12), 7973–8001. Retrieved
909 from <https://acp.copernicus.org/articles/19/7973/2019/> doi:
910 10.5194/acp-19-7973-2019
- 911 Doughty, C. E., Flanner, M. G., & Goulden, M. L. (2010). Effect of smoke on
912 subcanopy shaded light, canopy temperature, and carbon dioxide uptake
913 in an Amazon rainforest. *Global Biogeochemical Cycles*, 24(3), 1–10. doi:
914 10.1029/2009GB003670
- 915 Doughty, C. E., Metcalfe, D. B., Girardin, C. A., Amézquita, F. F., Cabrera,
916 D. G., Huasco, W. H., ... Malhi, Y. (2015). Drought impact on forest
917 carbon dynamics and fluxes in Amazonia. *Nature*, 519(7541), 78–82. doi:
918 10.1038/nature14213
- 919 Finnigan, J. (2006). The storage term in eddy flux calculations. *Agricultural and*
920 *Forest Meteorology*, 136(3-4), 108–113. doi: 10.1016/j.agrformet.2004.12.010
- 921 Foken, T. (2008). *Micrometeorology*. Springer Berlin Heidelberg. doi: 10.1007/978-3
922 -540-74666-9
- 923 Freedman, J., Fitzjarrald, D., Moore, K., & Sakai, R. (1998). Boundary layer cloud
924 climatology and enhanced forest-atmosphere exchange. In *Preprints of 23rd*
925 *conference on agricultural and forest meteorology* (pp. 41–44).
- 926 Fu, Z., Gerken, T., Bromley, G., Araújo, A., Bonal, D., Burban, B., ... Stoy, P. C.
927 (2018). The surface-atmosphere exchange of carbon dioxide in tropical rain-
928 forests: Sensitivity to environmental drivers and flux measurement method-
929 ology. *Agricultural and Forest Meteorology*, 263(December 2017), 292–307.
930 Retrieved from <https://doi.org/10.1016/j.agrformet.2018.09.001> doi:
931 10.1016/j.agrformet.2018.09.001
- 932 Gao, Y. (2020). Atmospheric Aerosols Elevated Ecosystem Productivity of a Poplar
933 Plantation in Beijing, 2 China.
- 934 Gates, D. M. (1980). *Biophysical Ecology*.
- 935 Gatti, L. V., Basso, L. S., Miller, J. B., Gloor, M., Gatti Domingues, L., Cas-
936 sol, H. L., ... Neves, R. A. (2021). Amazonia as a carbon source linked
937 to deforestation and climate change. *Nature*, 595(7867), 388–393. Re-
938 trieved from <http://dx.doi.org/10.1038/s41586-021-03629-6> doi:
939 10.1038/s41586-021-03629-6
- 940 Gatti, L. V., Gloor, M., Miller, J. B., Doughty, C. E., Malhi, Y., Domingues, L. G.,
941 ... Lloyd, J. (2014). Drought sensitivity of Amazonian carbon balance re-
942 vealed by atmospheric measurements. *Nature*, 506(7486), 76–80. Retrieved
943 from <http://dx.doi.org/10.1038/nature12957> doi: 10.1038/nature12957
- 944 Goulden, M. L., Miller, S. D., Da Rocha, H. R., Menton, M. C., De Freitas, H. C., E
945 Silva Figueira, A. M., & Dias De Sousa, C. A. (2004). Diel and seasonal pat-
946 terns of tropical forest CO₂ exchange. *Ecological Applications*, 14(4 SUPPL.),
947 42–54. doi: 10.1890/02-6008
- 948 Grace, J., Malhi, Y., Lloyd, J., McIntyre, J., Miranda, A. C., Meir, P., & Miranda,
949 H. S. (1996). The use of eddy covariance to infer the net carbon dioxide
950 uptake of Brazilian rain forest. *Global Change Biology*, 2(3), 209–217. doi:

- 10.1111/j.1365-2486.1996.tb00073.x
- 951 Gu, L., Fuentes, J. D., Garstang, M., Silva, J. T. D., Heitz, R., Sigler, J., & Shugart,
952 H. H. (2001). Cloud modulation of surface solar irradiance at a pasture site in
953 Southern Brazil. *Agricultural and Forest Meteorology*, *106*(2), 117–129. doi:
954 10.1016/S0168-1923(00)00209-4
- 955 Gu, L., Fuentes, J. D., Shugart, H. H., Staebler, R. M., & Black, T. A. (1999). Re-
956 sponses of net ecosystem exchanges of carbon dioxide to changes in cloudiness:
957 Results from two North American deciduous forests. *Journal of Geophysical*
958 *Research Atmospheres*, *104*(D24), 31421–31434. doi: 10.1029/1999JD901068
- 959 Helliker, B. R., & Ehleringer, J. R. (2000). Establishing a grassland signature in
960 veins: $\delta^{18}\text{O}$ in the leaf water of C_3 and C_4
961 grasses. *Proceedings of the National Academy of Sciences*, *97*(14), 7894–7898.
962 Retrieved from <https://www.pnas.org/doi/abs/10.1073/pnas.97.14.7894>
963 doi: 10.1073/pnas.97.14.7894
- 964 Hofhansl, F., Andersen, K. M., Fleischer, K., Fuchslueger, L., Rammig, A., Schaap,
965 K. J., ... Lapola, D. M. (2016). Amazon forest ecosystem responses to ele-
966 vated atmospheric CO_2 and alterations in nutrient availability: Filling the gaps
967 with model-experiment integration. *Frontiers in Earth Science*, *4*(February),
968 1–9. doi: 10.3389/feart.2016.00019
- 969 Holben, B. N., Eck, T. F., Slutsker, I., Tanré, D., Buis, J. P., Setzer, A., ...
970 Smirnov, A. (1998). AERONET - A federated instrument network and data
971 archive for aerosol characterization. *Remote Sensing of Environment*, *66*(1),
972 1–16. doi: 10.1016/S0034-4257(98)00031-5
- 973 Hollinger, D. Y., & Richardson, A. D. (2005). Uncertainty in eddy covariance mea-
974 surements and its application to physiological models. , 873–885.
- 975 Huntingford, C., Zelazowski, P., Galbraith, D., Mercado, L. M., Sitch, S., Fisher,
976 R., ... Cox, P. M. (2013). Simulated resilience of tropical rainforests to CO_2
977 -induced climate change. *Nature Geoscience*, *6*(4), 268–273. Retrieved from
978 <http://dx.doi.org/10.1038/ngeo1741> doi: 10.1038/ngeo1741
- 979 Jing, X., Huang, J., Wang, G., Higuchi, K., Bi, J., Sun, Y., ... Wang, T. (2010).
980 The effects of clouds and aerosols on net ecosystem CO_2 exchange over semi-
981 arid Loess Plateau of Northwest China. *Atmospheric Chemistry and Physics*,
982 *10*(17), 8205–8218. doi: 10.5194/acp-10-8205-2010
- 983 Kanniah, K. D., Beringer, J., North, P., & Hutley, L. (2012). Control of at-
984 mospheric particles on diffuse radiation and terrestrial plant productiv-
985 ity: A review. *Progress in Physical Geography*, *36*(2), 209–237. doi:
986 10.1177/0309133311434244
- 987 Koren, I., Dagan, G., & Altaratz, O. (2014). From aerosol-limited to invigoration of
988 warm convective clouds. *Science*, *344*(6188), 1143–1146. doi: 10.1126/science
989 .1252595
- 990 Levy, R. C., Mattoo, S., Munchak, L. A., Remer, L. A., Sayer, A. M., Patadia, F.,
991 & Hsu, N. C. (2013). The Collection 6 MODIS aerosol products over land
992 and ocean. *Atmospheric Measurement Techniques*, *6*(11), 2989–3034. doi:
993 10.5194/amt-6-2989-2013
- 994 Lorenzi, H. (2000). *Arvores , brasileiras*. São Paulo.
- 995 Lorenzi, H. (2002). *Arvores , brasileiras* (L. Instituto Plantarum de Estudos da
996 Flora, Ed.). Sao Paulo.
- 997 Malavelle, F. F., Haywood, J. M., Mercado, L. M., Folberth, G. A., Bellouin, N.,
998 Sitch, S., & Artaxo, P. (2019). Studying the impact of biomass burning aerosol
999 radiative and climate effects on the Amazon rainforest productivity with an
1000 Earth system model. *Atmospheric Chemistry and Physics*, *19*(2), 1301–1326.
1001 doi: 10.5194/acp-19-1301-2019
- 1002 Malhi, Y., Melack, J., Gatti, L. V., Ometto, J. P., Kesselmeier, J., Wolff, S., ...
1003 Silva Junior, C. H. L. (2021). *Chapter 6: Biogeochemical Cycles in the Ama-*
1004 *zon*. doi: 10.55161/takr3454
- 1005

- 1006 Martin, S. T., Andreae, M. O., Althausen, D., Artaxo, P., Baars, H., Borrmann, S.,
 1007 ... Zorn, S. R. (2010). An overview of the Amazonian Aerosol Characteri-
 1008 zation Experiment 2008 (AMAZE-08). *Atmospheric Chemistry and Physics*,
 1009 10(23), 11415–11438. doi: 10.5194/acp-10-11415-2010
- 1010 Martin, S. T., Andreae, M. O., Artaxo, P., Baumgardner, D., Chen, Q., Goldstein,
 1011 A. H., ... Trebs, I. (2010). Sources and properties of Amazonian aerosol
 1012 particles. *Reviews of Geophysics*, 48(2). doi: 10.1029/2008RG000280
- 1013 MATLAB. (2013). *version 9.8.8.748 (r2013a)*. Natick, Massachusetts: The Math-
 1014 Works Inc.
- 1015 Mercado, L. M., Bellouin, N., Sitch, S., Boucher, O., Huntingford, C., Wild, M., &
 1016 Cox, P. M. (2009). Impact of changes in diffuse radiation on the global land
 1017 carbon sink. *Nature*, 458(7241), 1014–1017. doi: 10.1038/nature07949
- 1018 Meyers, T. P., & Dale, R. F. (1983). *Predicting daily insolation with hourly cloud*
 1019 *height and coverage*. (Vol. 22) (No. 4). doi: 10.1175/1520-0450(1983)022<0537:
 1020 PDIWHC>2.0.CO;2
- 1021 Min, Q. (2005). Impacts of aerosols and clouds on forest-atmosphere carbon ex-
 1022 change. *Journal of Geophysical Research: Atmospheres*, 110(D6). Retrieved
 1023 from [https://agupubs.onlinelibrary.wiley.com/doi/abs/10.1029/
 1024 2004JD004858](https://agupubs.onlinelibrary.wiley.com/doi/abs/10.1029/2004JD004858) doi: <https://doi.org/10.1029/2004JD004858>
- 1025 Moncrieff, J. B., Massheder, J. M., De Bruin, H., Elbers, J., Friborg, T.,
 1026 Heusinkveld, B., ... Verhoef, A. (1997). A system to measure surface fluxes
 1027 of momentum, sensible heat, water vapour and carbon dioxide. *Journal of*
 1028 *Hydrology*, 188-189(1-4), 589–611. doi: 10.1016/S0022-1694(96)03194-0
- 1029 Montagnani, L., Grünwald, T., Kowalski, A., Mammarella, I., Merbold, L., Metzger,
 1030 S., ... Siebicke, L. (2018). Estimating the storage term in eddy covariance
 1031 measurements: The ICOS methodology. *International Agrophysics*, 32(4),
 1032 551–567. doi: 10.1515/intag-2017-0037
- 1033 Moreira, D. S., Freitas, S. R., Bonatti, J. P., Mercado, L. M., É. Rosário, N. M.,
 1034 Longo, K. M., ... Gatti, L. V. (2013). Coupling between the JULES land-
 1035 surface scheme and the CCATT-BRAMS atmospheric chemistry model
 1036 (JULES-CCATT-BRAMS1.0): Applications to numerical weather forecast-
 1037 ing and the CO2 budget in South America. *Geoscientific Model Development*,
 1038 6(4), 1243–1259. doi: 10.5194/gmd-6-1243-2013
- 1039 Moreira, D. S., Longo, K. M., Freitas, S. R., Yamasoe, M. A., Mercado, L. M.,
 1040 Rosário, N. E., ... Correia, C. C. (2017). Modeling the radiative ef-
 1041 fects of biomass burning aerosols on carbon fluxes in the Amazon re-
 1042 gion. *Atmospheric Chemistry and Physics*, 17(23), 14785–14810. doi:
 1043 10.5194/acp-17-14785-2017
- 1044 Morgan, W. T., Darbyshire, E., Spracklen, D. V., Artaxo, P., & Coe, H. (2019).
 1045 Non-deforestation drivers of fires are increasingly important sources of aerosol
 1046 and carbon dioxide emissions across Amazonia. *Scientific Reports*, 9(1), 1–15.
 1047 Retrieved from <http://dx.doi.org/10.1038/s41598-019-53112-6> doi:
 1048 10.1038/s41598-019-53112-6
- 1049 Murphy, P. G., & Lugo, A. E. (1986). Ecology of tropical dry forest. *Annual re-*
 1050 *view of ecology and systematics*. Vol. 17(November 2003), 67–88. doi: 10.1146/
 1051 annurev.es.17.110186.000435
- 1052 Nagy, L., Artaxo, P., & Forsberg, B. R. (2016). *Interactions Between Biosphere, At-*
 1053 *mosphere, and Human Land Use in the Amazon Basin: An Introduction*. doi:
 1054 10.1007/978-3-662-49902-3_1
- 1055 Nagy, R. C., Porder, S., Brando, P., Davidson, E. A., Figueira, A. M. e. S., Neill,
 1056 C., ... Trumbore, S. (2018). Soil carbon dynamics in soybean cropland
 1057 and forests in mato grosso, brazil. *Journal of Geophysical Research: Biogeo-*
 1058 *sciences*, 123(1), 18–31. Retrieved from [https://agupubs.onlinelibrary
 1059 .wiley.com/doi/abs/10.1002/2017JG004269](https://agupubs.onlinelibrary.wiley.com/doi/abs/10.1002/2017JG004269) doi: [https://doi.org/10.1002/
 1060 2017JG004269](https://doi.org/10.1002/2017JG004269)

- 1061 Nepstad, D., McGrath, D., Stickler, C., Alencar, A., Azevedo, A., Swette, B., ...
 1062 Hess, L. (2014). Slowing Amazon deforestation through public policy and
 1063 interventions in beef and soy supply chains. *Science*, *344*(6188), 1118–1123.
 1064 doi: 10.1126/science.1248525
- 1065 Niyogi, D., Chang, H. I., Saxena, V. K., Holt, T., Alapaty, K., Booker, F., ... Xue,
 1066 Y. (2004). Direct observations of the effects of aerosol loading on net ecosys-
 1067 tem CO₂ exchanges over different landscapes. *Geophysical Research Letters*,
 1068 *31*(20), 1–5. doi: 10.1029/2004GL020915
- 1069 Nogueira, E. M., Nelson, B. W., Fearnside, P. M., França, M. B., & de Oliveira,
 1070 Á. C. A. (2008). Tree height in Brazil's 'arc of deforestation': Shorter trees
 1071 in south and southwest Amazonia imply lower biomass. *Forest Ecology and*
 1072 *Management*, *255*(7), 2963–2972. doi: 10.1016/j.foreco.2008.02.002
- 1073 Oliveira, P. H., Artaxo, P., Pires, C., De Lucca, S., Procópio, A., Holben, B., ...
 1074 Rocha, H. R. (2007). The effects of biomass burning aerosols and clouds on
 1075 the CO₂ flux in Amazonia. *Tellus, Series B: Chemical and Physical Meteorol-*
 1076 *ogy*, *59*(3), 338–349. doi: 10.1111/j.1600-0889.2007.00270.x
- 1077 Oliveira-Filho AT, R. J., & Oliveira. (2002). *The Cerrados of Brazil* (Vol. 20)
 1078 (No. 11). Nova York. doi: 10.1258/ijsa.2009.009019
- 1079 Pan, Y. (2011). A large and persistent carbon sink in the world's forests. *Science*,
 1080 *333*(August), 988–993.
- 1081 Prado, D. E., & Gibbs, P. E. (1993). Patterns of Species Distributions in the Dry
 1082 Seasonal Forests of South America. *Annals of the Missouri Botanical Garden*,
 1083 *80*(4), 902. doi: 10.2307/2399937
- 1084 Procopio, A. S., Artaxo, P., Kaufman, Y. J., Remer, L. A., Schafer, J. S., & Hol-
 1085 ben, B. N. (2004). Multiyear analysis of amazonian biomass burning smoke
 1086 radiative forcing of climate. *Geophysical Research Letters*, *31*(3), 1–4. doi:
 1087 10.1029/2003GL018646
- 1088 Rap, A. (2015). Fires increase Amazon forest productivity. *Geophysical Research*
 1089 *Letters* (June), 4654–4662. doi: 10.1002/2015GL063719. Received
- 1090 Rap, A., Scott, C. E., Reddington, C. L., Mercado, L., Ellis, R. J., Garraway, S., ...
 1091 Spracklen, D. V. (2018). Enhanced global primary production by biogenic
 1092 aerosol via diffuse radiation fertilization. *Nature Geoscience*, *11*(9), 640–644.
 1093 Retrieved from <http://dx.doi.org/10.1038/s41561-018-0208-3> doi:
 1094 10.1038/s41561-018-0208-3
- 1095 Ratter, J. A., Askew, G. P., Montgomery, R. F., & Gifford, D. R. (1978). Obser-
 1096 vations on the vegetation of northeastern Mato Grosso II. Forests and soils of
 1097 the Rio Suiá–Missu area. *Proceedings of the Royal Society of London. Series*
 1098 *B, Containing papers of a Biological character. Royal Society (Great Britain)*,
 1099 *203*(1151), 191–208. doi: 10.1098/rspb.1978.0100
- 1100 Reindl, D., Beckman, W., & Duffie, J. (1990). Diffuse fraction correlations. *So-*
 1101 *lar Energy*, *45*(1), 1–7. Retrieved from [https://www.sciencedirect.com/](https://www.sciencedirect.com/science/article/pii/0038092X9090060P)
 1102 [science/article/pii/0038092X9090060P](https://www.sciencedirect.com/science/article/pii/0038092X9090060P) doi: [https://doi.org/10.1016/](https://doi.org/10.1016/0038-092X(90)90060-P)
 1103 [0038-092X\(90\)90060-P](https://doi.org/10.1016/0038-092X(90)90060-P)
- 1104 Remer, L. A., Kaufman, Y. J., Tanré, D., Mattoo, S., Chu, D. A., Martins, J. V.,
 1105 ... Holben, B. N. (2005). The MODIS aerosol algorithm, products, and
 1106 validation. *Journal of the Atmospheric Sciences*, *62*(4), 947–973. doi:
 1107 10.1175/JAS3385.1
- 1108 Remer, L. A., Mattoo, S., Levy, R. C., & Munchak, L. A. (2013). MODIS 3 km
 1109 aerosol product: Algorithm and global perspective. *Atmospheric Measurement*
 1110 *Techniques*, *6*(7), 1829–1844. doi: 10.5194/amt-6-1829-2013
- 1111 Saatchi, S. S., Harris, N. L., Brown, S., Lefsky, M., Mitchard, E. T., Salas, W., ...
 1112 Morel, A. (2011). Benchmark map of forest carbon stocks in tropical regions
 1113 across three continents. *Proceedings of the National Academy of Sciences of the*
 1114 *United States of America*, *108*(24), 9899–9904. doi: 10.1073/pnas.1019576108
- 1115 Saraiva, I., Silva Dias, M. A., Morales, C. A., & Saraiva, J. M. (2016). Regional

- 1116 variability of rain clouds in the amazon basin as seen by a network of weather
1117 radars. *Journal of Applied Meteorology and Climatology*, 55(12), 2657–2675.
1118 doi: 10.1175/JAMC-D-15-0183.1
- 1119 Schafer, J. S., Eck, T. F., Holben, B. N., Artaxo, P., & Duarte, A. F. (2008). Char-
1120 acterization of the optical properties of atmospheric aerosols in Amazônia
1121 from long-term AERONET monitoring (1993-1995 and 1999-2006). *Journal of*
1122 *Geophysical Research Atmospheres*, 113(4), 1–16. doi: 10.1029/2007JD009319
- 1123 Schafer, J. S., Eck, T. F., Holben, B. N., Artaxo, P., Yamasoe, M. A., & Procopio,
1124 A. S. (2002). Observed reductions of total solar irradiance by biomass-burning
1125 aerosols in the Brazilian Amazon and Zambian Savanna. *Geophysical Research*
1126 *Letters*, 29(17), 2–5. doi: 10.1029/2001GL014309
- 1127 Schafer, J. S., Holben, B. N., Eck, T. F., Yamasoe, M. A., & Artaxo, P. (2002).
1128 Atmospheric effects on insolation in the Brazilian Amazon: Observed mod-
1129 ification of solar radiation by clouds and smoke and derived single scatter-
1130 ing albedo of fire aerosols. *Journal of Geophysical Research: Atmospheres*,
1131 107(20), LBA 41–1–LBA 41–15. doi: 10.1029/2001JD000428
- 1132 Schuepp, P. H., Leclerc, M. Y., MacPherson, J. I., & Desjardins, R. L. (1990).
1133 Footprint prediction of scalar fluxes from analytical solutions of the dif-
1134 fusion equation. *Boundary-Layer Meteorology*, 50(1-4), 355–373. doi:
1135 10.1007/BF00120530
- 1136 Shilling, J. E., Pekour, M. S., Fortner, E. C., Artaxo, P., de Sá, S., Hubbe, J. M.,
1137 ... Wang, J. (2018). Aircraft observations of the chemical composition
1138 and aging of aerosol in the manaus urban plume during goamazon 2014/5.
1139 *Atmospheric Chemistry and Physics*, 18(14), 10773–10797. Retrieved
1140 from <https://acp.copernicus.org/articles/18/10773/2018/> doi:
1141 10.5194/acp-18-10773-2018
- 1142 Silva, C. V., Aragão, L. E., Young, P. J., Espirito-Santo, F., Berenguer, E., Ander-
1143 son, L. O., ... Barlow, J. (2020). Estimating the multi-decadal carbon deficit
1144 of burned Amazonian forests. *Environmental Research Letters*, 15(11). doi:
1145 10.1088/1748-9326/abb62c
- 1146 Spitters, C. J., Toussaint, H. A., & Goudriaan, J. (1986). Separating the diffuse and
1147 direct component of global radiation and its implications for modeling canopy
1148 photosynthesis Part I. Components of incoming radiation. *Agricultural and*
1149 *Forest Meteorology*, 38(1-3), 217–229. doi: 10.1016/0168-1923(86)90060-2
- 1150 Tribuzy, E. S. (2005). Canopy leaf temperature variations and their effect on the
1151 CO₂ assimilation rate in Central Amazonia (in Portuguese). *Doctoral thesis*,
1152 102.
- 1153 von Randow, C., Manzi, A. O., Kruijt, B., de Oliveira, P. J., Zanchi, F. B., Silva,
1154 R. L., ... Kabat, P. (2004). Comparative measurements and seasonal
1155 variations in energy and carbon exchange over forest and pasture in South
1156 West Amazonia. *Theoretical and Applied Climatology*, 78(1-3), 5–26. doi:
1157 10.1007/s00704-004-0041-z
- 1158 Vourlitis, G. L., De Almeida Lobo, F., Zeilhofer, P., & De Souza Nogueira, J. (2011).
1159 Temporal patterns of net CO₂ exchange for a tropical semideciduous forest of
1160 the southern Amazon Basin. *Journal of Geophysical Research: Biogeosciences*,
1161 116(3), 1–15. doi: 10.1029/2010JG001524
- 1162 Vourlitis, G. L., Priante Filho, N., Hayashi, M. M., Nogueira, J. D. S., Caseiro,
1163 F. T., & Campelo, J. H. (2002). Seasonal variations in the evapotranspira-
1164 tion of a transitional tropical forest of Mato Grosso, Brazil. *Water Resources*
1165 *Research*, 38(6), 30–1–30–11. doi: 10.1029/2000wr000122
- 1166 Vourlitis, G. L., Priante Filho, N., Hayashi, M. M., Nogueira, J. D. S., Caseiro,
1167 F. T., & Holanda Campelo, J. (2001). Seasonal variations in the net ecosystem
1168 CO₂ exchange of a mature Amazonian transitional tropical forest (cerradão).
1169 *Functional Ecology*, 15(3), 388–395. doi: 10.1046/j.1365-2435.2001.00535.x
- 1170 Wang, X., Wang, C., Wu, J., Miao, G., Chen, M., Chen, S., ... Liu, L. (2021). In-

- 1171 intermediate aerosol loading enhances photosynthetic activity of croplands. *Geo-*
1172 *physical Research Letters*, 48(7), e2020GL091893. Retrieved from [https://](https://agupubs.onlinelibrary.wiley.com/doi/abs/10.1029/2020GL091893)
1173 agupubs.onlinelibrary.wiley.com/doi/abs/10.1029/2020GL091893
1174 (e2020GL091893 2020GL091893) doi: <https://doi.org/10.1029/2020GL091893>
- 1175 Wang, Z., Wang, C., Wang, X., Wang, B., Wu, J., & Liu, L. (2022). Aerosol
1176 pollution alters the diurnal dynamics of sun and shade leaf photosynthesis
1177 through different mechanisms. *Plant, Cell & Environment*, 45(10), 2943-
1178 2953. Retrieved from [https://onlinelibrary.wiley.com/doi/abs/10.1111/](https://onlinelibrary.wiley.com/doi/abs/10.1111/pce.14411)
1179 [pce.14411](https://onlinelibrary.wiley.com/doi/abs/10.1111/pce.14411) doi: <https://doi.org/10.1111/pce.14411>
- 1180 Yakir, D. (2003). 4.07 - the stable isotopic composition of atmospheric co₂. In
1181 H. D. Holland & K. K. Turekian (Eds.), *Treatise on geochemistry* (p. 175-
1182 212). Oxford: Pergamon. Retrieved from [https://www.sciencedirect.com/](https://www.sciencedirect.com/science/article/pii/B008043751604038X)
1183 [science/article/pii/B008043751604038X](https://www.sciencedirect.com/science/article/pii/B008043751604038X) doi: [https://doi.org/10.1016/](https://doi.org/10.1016/B0-08-043751-6/04038-X)
1184 [B0-08-043751-6/04038-X](https://doi.org/10.1016/B0-08-043751-6/04038-X)
- 1185 Yamasoe, M. A., Randow, C. V., Manzi, A. O., Schafer, J. S., Eck, T. F., & Holben,
1186 B. N. (2006). Effect of smoke and clouds on the transmissivity of photosyn-
1187 thetically active radiation inside the canopy. , 1645–1656.
- 1188 Yuan, W., Zheng, Y., Piao, S., Ciais, P., Lombardozzi, D., Wang, Y., ... Yang, S.
1189 (2019). Increased atmospheric vapor pressure deficit reduces global vegetation
1190 growth. *Science Advances*, 5(8), 1–13. doi: 10.1126/sciadv.aax1396
- 1191 Zhang, M., Yu, G. R., Zhang, L. M., Sun, X. M., Wen, X. F., Han, S. J., & Yan,
1192 J. H. (2010). Impact of cloudiness on net ecosystem exchange of carbon
1193 dioxide in different types of forest ecosystems in China. *Biogeosciences*, 7(2),
1194 711–722. doi: 10.5194/bg-7-711-2010